

Modeling the large-scale power deficit

Sandro D. P. Vitenti,^{1,2,*} Patrick Peter,^{3,4,†} and Antony Valentini^{5,6,‡}

¹*Instituto de Física – Universidade de Brasília, Brazil.*

²*Centre for Cosmology, Particle Physics and Phenomenology,
Institute of Mathematics and Physics, Louvain University,
2 Chemin du Cyclotron, 1348 Louvain-la-Neuve, Belgium.*

³*Institut d’Astrophysique de Paris and Institut Lagrange de Paris
CNRS (UMR 7095) and Sorbonne Université, 98 bis boulevard Arago, 75014 Paris, France.*

⁴*Department of Applied Mathematics and Theoretical Physics,
Centre for Mathematical Sciences, University of Cambridge,
Wilberforce Road, Cambridge CB3 0WA, United Kingdom.*

⁵*Augustus College, 14 Augustus Road, London SW19 6LN, United Kingdom.*

⁶*Department of Physics and Astronomy, Clemson University,
Kinard Laboratory, Clemson, SC 29634-0978, USA.*

(Dated: May 2, 2022)

We investigate a set of cosmological models for which the primordial power spectrum has a large-scale power deficit. The standard power-law spectrum is subject to long-wavelength modifications described by some new parameters, resulting in corrections to the anisotropies in the cosmic microwave background. The new parameters are fitted to different data sets: temperature only, temperature and polarization, the low-redshift determination of H_0 , and baryonic acoustic oscillations. We discuss the statistical significance of the modified spectra, from both frequentist and Bayesian perspectives. Our analysis suggests motivations for considering models that break scalar-tensor consistency, or models with negligible power in the far super-Hubble limit. We present what appears to be substantial evidence for a new scale around 350 Mpc above which the primordial (scalar) power spectrum is sharply reduced by about 20%.

I. INTRODUCTION

Cosmological data is now accumulating at such a rate that the phrase ‘precision cosmology’ is often used to describe our current understanding of the primordial universe [1]. As is well known, the largest scales show features whose significance is unclear and which remain controversial [2]. In particular, the existence or otherwise of a large-scale power deficit remains an open question. A natural way to address this, explored in the present paper, is to postulate that the primordial power spectrum is suppressed at large scales by some as-yet-unknown physical mechanism [3]. Assuming a phenomenological parameterization of the modification, which we shall from now on refer to as a deficit function, we may then analyze the available data and evaluate the statistical significance of any proposed modified spectrum.

A first analysis of data from the cosmic microwave background (CMB) was carried out by the Planck team [4], specifically for their temperature and polarization data. They considered two modifications of the primordial power spectrum, both involving two extra parameters and suppressing power on large scales. They concluded that ‘*neither of these two models with two extra parameters is preferred over the base Λ CDM model*’.

The purpose of this paper is to re-examine these con-

clusions by considering a wider set of possible deficit functions together with a wider set of cosmological data – specifically including the low-redshift determination of H_0 (leading to $H_0 = 73.24 \pm 1.74 \text{ km} \cdot \text{s}^{-1} \cdot \text{Mpc}^{-1}$ which is in tension with the Planck result $H_0^{\text{Planck}} \sim 67.3 \text{ km} \cdot \text{s}^{-1} \cdot \text{Mpc}^{-1}$) and the Baryonic Acoustic Oscillations (BAO).

In our original motivating model for a physical large-scale power deficit, the primordial perturbations are produced in a pre-inflationary radiation-dominated phase [5] that is in a state of ‘quantum nonequilibrium’ [6–8] (resulting in violations of the usual Born rule, a possibility that is allowed in the de Broglie-Bohm pilot-wave formulation of quantum mechanics [9]). Dynamical relaxation to quantum equilibrium (that is, to the Born rule) is found to be suppressed at very large wavelengths, thereby naturally producing a dip in the primordial power spectrum at large scales. If we add the simplifying assumption that the spectrum is unchanged by the transition from pre-inflation to inflation, we obtain a three-parameter modification of the CMB spectrum (noting that quantum relaxation may be shown to not take place during inflation itself [9]). In this paper we extend the modification to four parameters in order to be able to compare with the cases studied by the Planck team.

We have found that temperature data combined with the low-redshift determination of H_0 and the baryon oscillations data (without polarization) are able to constrain two of the new parameters fairly well, yielding a moderate improvement at the 2.41σ level in favor of our quantum relaxation model (in particular for the combina-

* sandro.vitenti@uclouvain.be

† peter@iap.fr

‡ antonyv@clemson.edu

tion of temperature data with H_0 alone). However, the significance of the fits tends to degrade when polarization data are added. We then seem driven to the conclusion that our starting point for a modified power spectrum yields statistically inconclusive results. Alternatively, however, peculiarities of the fit when polarization data are added suggest that a better fit might be obtained in a model that allows for a breaking of scalar-tensor consistency. Our analysis suggests a motivation for considering such models, which arise naturally in quantum relaxation scenarios. Our results also suggest a motivation for considering models with negligible power in the far super-Hubble limit.

In the course of our analysis we found that the fitting process led naturally to a preference for an extreme case of our (scalar) deficit function. The best fit seems to be obtained with a simple two-parameter sharp decrease in the power spectrum, with a statistical significance ranging from substantial to strong. We find a good account of the data with a sudden dip of about 20% at a characteristic scale of around 350 Mpc. Whether or not this provides a new physically-relevant scale in other areas of cosmology is left for future investigation.

In Section II we present our cosmological model and our parameterizations of the modified power spectrum. In Section III we describe the methodology for our statistical data analysis. Our numerical approach is summarized in Section IV. Our results are presented and discussed in detail in Section V. A possible breaking of scalar-tensor consistency is briefly addressed in Section V C. The implications of our results for future work on quantum relaxation scenarios are summarized in Section VI. The significance and properties of the sudden jump deficit function are discussed in Section VII. Our conclusions are drawn in Section VIII. These are followed by two appendices. Appendix A discusses the cosmology library used in our numerical analysis, while Appendix B provides more details of our data analysis.

II. COSMOLOGICAL MODEL

Even though the CMB anisotropies depend strongly on the primordial power spectrum (PPS), they also depend on other aspects of the cosmological model which are unrelated to the origin of the primordial perturbations. For this reason, we start by specifying the complete cosmological model that we use to calculate the CMB anisotropies theoretically.

A. Deficit functions

In what follows we do not adopt a particular inflationary model (or any reasonable alternative one might consider [10–12]) but only a simple power-law model of the fiducial power spectrum as best fitted by all currently available data. We also assume, again in accordance with

known data, that only the adiabatic mode is present. We do not consider any contribution from gravitational waves. In such a framework, all the information about the primordial perturbations is contained in the fiducial power spectrum

$$\mathcal{P}_F(k) = \mathcal{P}_{\text{plaw}}(k) \equiv \mathcal{A}_s \left(\frac{k}{k_*} \right)^{n_s-1}, \quad (1)$$

where k_* is the pivotal mode chosen (following the Planck analysis) to be $k_* = 0.05 \text{ Mpc}^{-1}$, \mathcal{A}_s is the amplitude of the adiabatic mode measured at k_* , and n_s is the spectral index. The modified power spectrum may then be described by a deficit function $\xi(k)$, or alternatively $\chi(k) \equiv 1 - \xi(k)$, defined by

$$\mathcal{P}(k) = \xi(k)\mathcal{P}_F(k) = [1 - \chi(k)]\mathcal{P}_F(k). \quad (2)$$

Here $\mathcal{P}(k)$ is the effective (estimated) power spectrum and $\lim_{k \gg k_c} \chi(k) = 0$ for some physical wavenumber k_c to be determined by the data. The fiducial power spectrum is modified on large scales ($k \ll k_c$) but not on small scales ($k \gg k_c$, where $\xi \rightarrow 1$). Note that this approach does not model the primordial mechanism in play [3] but merely assumes a phenomenological form for the resulting spectrum.

Refs. [13, 14] considered two phenomenological models of the CMB power deficit at low multipoles. The first is the so-called exponential cut-off [15], which we modify slightly to include the possibility of a large-scale renormalization:

$$\chi_{\text{exp}}(k) = 1 - \xi_{\text{exp}}(k) = (1 - \beta) \exp \left[- \left(\frac{k}{k_c} \right)^\lambda \right], \quad (3)$$

where k_c explicitly controls the cut-off wavelength that was implicit in (2), λ provides a transition rate, and β is introduced to mimic the large-scale behavior of our more general model (given below). This parameterization indeed leaves the small scales unchanged: $\lim_{k \gg k_c} \chi_{\text{exp}}(k) = 0$. For the large-scale limit we obtain

$$\xi_{\text{exp}}(k) \underset{k \ll k_c}{\approx} \beta + (1 - \beta) \left(\frac{k}{k_c} \right)^\lambda,$$

so that for $\beta \neq 0$ the spectrum is merely rescaled by the constant β . On the other hand, when $\beta = 0$ (as in the original study by the Planck team) the power spectrum becomes

$$\mathcal{P}(k) \underset{k \ll k_c}{\approx} \left(\frac{k_*}{k_c} \right)^\lambda \mathcal{A}_s \left(\frac{k}{k_*} \right)^{n_s+\lambda-1}. \quad (4)$$

This expression adds freedom (at large scales) to the spectral index through the parameter λ , which at the same time controls the transition rate and the large-scale power-law behavior. In the following we employ three different choices of parameter sets: **expc3**, which labels the model with all the parameters (k_c , λ , β) freely varying,

expc2 where we set $\beta = 0$, and **expc1** where in addition to $\beta = 0$ we impose the further constraint $\lambda = \frac{1}{2}$.

The second model introduced in Ref. [14] consists of a broken power law:

$$\xi_{\text{bpl}}(k) = \begin{cases} \left(\frac{k}{k_c}\right)^\lambda & \text{for } k \leq k_c, \\ 1 & \text{for } k \geq k_c. \end{cases} \quad (5)$$

We shall refer to this single parameterization, with both parameters k_c and λ freely varying, as **bpl**.

A more general parameterization has been obtained in the framework of quantum nonequilibrium initial conditions [9]. In this setting one assumes that the quantum wave functional is the usual vacuum, but the actual field variables take values whose variance is smaller than the usual quantum variance (a feature that is possible in the de Broglie-Bohm formulation of quantum mechanics). If some fluctuations exit the Hubble scale while still in a nonequilibrium state, they may be stuck with a low-variance distribution until they become classical. To obtain a prediction, Ref. [6] considered quantum relaxation (from initial nonequilibrium) for a spectator scalar field during a pre-inflationary radiation-dominated phase and calculated the resulting power spectrum. Adding the simplifying assumption that the spectrum is unchanged during the transition from pre-inflation to inflation, a ‘quantum relaxation’ deficit function $\xi_{\text{neq}}(k) = 1 - \chi_{\text{neq}}(k)$ was found which, after generalizing from a fixed index $\lambda = 1$ to an arbitrary index λ , reads¹

$$\chi_{\text{neq}}(k) = \alpha \left\{ \frac{\pi}{2} - \arctan \left[\left(\frac{k}{k_c} \right)^\lambda + b \right] \right\}. \quad (6)$$

The parameter b is constrained by the physical requirement that $\xi_{\text{neq}}(k) > 0$ for all k . In the limit $k \rightarrow 0$ this requires

$$b > \tan \left(\frac{\pi}{2} - \frac{1}{\alpha} \right)$$

to avoid the spectrum becoming negative. As before the parameters α and λ as well as the characteristic scale k_c must be positive definite. While the latter three constraints are mostly harmless, the condition on b presents a challenge. Dealing with such a constrained parameter space is often impractical when performing a statistical analysis, and we therefore avoid it by introducing a new parameter β defined implicitly by

$$b(\alpha, \beta) \equiv \tan \left(\frac{\pi}{2} - \frac{|1 - \beta|}{\alpha} \right). \quad (7)$$

¹ To connect with the notation of Ref. [6], the coefficient there denoted c_3 is equal to our $1/\alpha$ while the function there denoted $\xi(k)$ is equal to our $\xi_{\text{neq}}(k)/\alpha$.

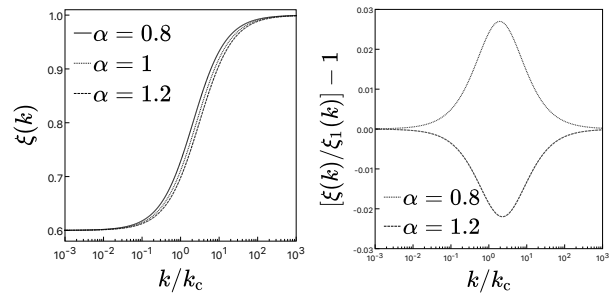


FIG. 1. Effect of the parameter α on $\xi(k)$ for $\beta = 0.6$ and $\lambda = 1$. The left panel shows the function $\xi_{\text{neq}}(k)$ for different values of α while the right panel exhibits the fractional difference from the fiducial with $\alpha = 1$. For the relevant range (see the fits below), the effect is at best of order a few percent.

The constraint on b may be recast as the simpler requirements

$$0 < \beta < 2, \quad 1 - \alpha\pi < \beta < 1 + \alpha\pi,$$

where the second one arises from the domain restriction of \tan . Finally we further simplify the constraints by imposing $\alpha > 1/\pi$, yielding the complete set

$$0 < \beta < 2, \quad \frac{1}{\pi} < \alpha, \quad 0 < \lambda.$$

The quantum relaxation deficit function $\xi_{\text{neq}}(k)$ now spans a simpler space which does not pose any serious numerical threat. It reads, explicitly,

$$\chi_{\text{neq}} = \text{sign}(1 - \beta) \alpha \left\{ \frac{\pi}{2} - \arctan \left[\left(\frac{k}{k_c} \right)^\lambda + b(\alpha, \beta) \right] \right\}. \quad (8)$$

A few examples are shown in Fig. 1, which also emphasizes that the parameter α does not play a very important role.

The deficit function (8) shares many properties with the Planck-exponential and broken-power laws. To begin with, the long-wavelength limit is

$$\lim_{k \rightarrow 0} \xi_{\text{neq}}(k) = \beta, \quad (9)$$

so that on large scales ($k \ll k_c$) we have

$$\mathcal{P}(k) \underset{k \ll k_c}{\approx} \beta \mathcal{A}_s \left(\frac{k}{k_\star} \right)^{n_s - 1}. \quad (10)$$

Thus $\xi_{\text{neq}}(k)$ behaves asymptotically like a step function that modifies the spectrum by multiplying it by β on large scales and leaving it unchanged on small scales.

The shape of the transition itself depends on both α and β , which in principle act independently. However, by plotting $\xi_{\text{neq}}(k)$ for different values of α (see Fig. 1) it is easy to see that varying α modifies $\xi_{\text{neq}}(k)$ only during the transition ($k \approx k_c$) and even then only slightly. Fig. 1 illustrates this for three values of α , specifically 0.8, 1.0

and 1.2 (and with $\beta = 0.6$), leading to a difference of at most $\approx 2\%$ in the transition region. We have also studied the difference for other values of β and for the most extreme cases ($\beta \ll 1$ and $\alpha > 1.5$ or $\alpha < 0.5$) we obtained a maximum difference of order $\lesssim 50\%$ at the transition point.

The additional index λ included in (8) permits two different effects. First, in the limit $\beta \rightarrow 0$ one finds

$$\xi_{\text{neq}}(k)|_{\beta \rightarrow 0} \underset{k \ll k_c}{\approx} \alpha \sin^2 \left(\frac{1}{\alpha} \right) \left(\frac{k}{k_c} \right)^\lambda. \quad (11)$$

For this choice of parameters the deficit function $\xi_{\text{neq}}(k)$ changes the spectral index by adding λ to the power of k . In other words, for large scales $\mathcal{P}(k \rightarrow 0) \propto k^{n_s + \lambda - 1}$ and we recover the large-scale behavior of the broken power law.

The second effect of λ is that it controls the rate of the transition between large and small scales, that is, how many decades it takes for $\xi_{\text{neq}}(k)$ to become approximately constant (numerically saturated to machine precision) for $k > k_c$ and $k < k_c$. For example, the left panel of Fig. 1 shows that $\xi_{\text{neq}}(k)$ is essentially constant as soon as $k/k_c \lesssim 10^{-2}$ or $k/k_c > 10^2$. The greater the value of λ , the faster the transition takes place. In fact – and this will play an important role in our analysis – in the limit $\lambda \gg 1$ and with $\beta \neq 0$ the deficit function becomes a step function and thus induces a sharp jump in the primordial power spectrum.

In short, using the final parametrization we have the following parameter space

$$(k_c, \lambda, \alpha, \beta).$$

The first parameter k_c sets the physical scale at which the transition occurs, λ controls the transition rate (and if $\beta = 0$ the broken power-law behavior), β represents the amplitude of the drop of the power-law spectrum, and α parameterizes the shape of the transition (although very weakly).

Given the precision with which the current data (see Refs.[13, 14]) can constrain the PPS, we consider three different regions of the parameter space. First we consider the entire space, which we call **atan4**, and fit all four parameters to the data (following the same nomenclature as for the cases above). In the second parametrization **atan3** we restrict attention to the subset $\lambda = 1$, so we measure only the position, the rescaling and the shape of the power-law modification. Next we additionally fix $\alpha = 1$, yielding the **atan2** parametrization with the shape parameter removed. Finally, in the fourth parameterization **atan1**, we keep $\lambda = 1$ and $\alpha = 1$ and we additionally impose $\beta = 0$, thus measuring only the transition point k_c . This last case, as discussed above, shares many characteristics with the broken power law.

When we consider models with some parameters fixed, this is akin to setting a very strong prior (essentially a delta function). Strictly speaking this should be done

only in the context of a well-defined theoretical framework. In a purely phenomenological description, it is important to note that results for such restricted models are only illustrative and their statistical significance should not be taken too literally. As we shall see, some of the restricted models perform comparatively well, but their significance might not necessarily be physically meaningful. In general, such restricted fits merely serve to test if a given data set is able to constrain a given parameter. From the results presented in the Tables, we see that for some data combinations all of the parameters are relevant (in the sense that leaving them unconstrained improves the fit), while for other data combinations the extra parameters are irrelevant (in the sense that leaving them unconstrained does not improve the fit). In an overall evaluation of the fits, we should avoid the risk of underestimating the p -values by considering p -values only for models with parameters that the data are actually able to constrain (as studied in detail below).

B. Λ CDM parameters

The rest of our adopted cosmology consists of the standard six-parameter Λ CDM model. We employ the same ingredients as those of Ref. [14], specifically:

- Hubble constant $H_0 = 100 h \text{ km} \cdot \text{s}^{-1} \cdot \text{Mpc}^{-1}$ (thereby defining h).
- Electromagnetic background radiation with a fixed temperature today $T_{\gamma 0} = 2.7255 \text{ K}$.
- One massive neutrino with $m_\nu = 0.06 \text{ eV}$, vanishing chemical potential, $T_{\nu 0} = 0.71611 T_{\gamma 0}$, and the effective massless neutrino number $N_{\text{eff}} = 2.0328$. This configuration is such that when the massive neutrino turns ultra-relativistic, the effective number of massless species is the standard 3.046.
- Cold dark matter density parameterized by $\Omega_{\text{cdm}} h^2$.
- Baryon matter density parameterized by $\Omega_b h^2$.
- Spatially flat model $\Omega_K = 0$.
- Instantaneous reionization with

$$\Delta_{\text{HeIII}} = \Delta_{\text{HII}} = 0.5, \quad \lambda_{\text{H}} = 3/2,$$

where λ_{H} is the reionization exponent and Δ_{HII} is the reionization width (for both $\text{HI} \rightarrow \text{HII}$ and $\text{HeI} \rightarrow \text{HeII}$) and Δ_{HeIII} is the width for $\text{HeII} \rightarrow \text{HeIII}$. The second reionization $\text{HeII} \rightarrow \text{HeIII}$ redshift is kept fixed at $z_{\text{HeIII}} = 3.5$. The first reionization redshift is employed as a free parameter z_{re} .

- The fiducial PPS of Eq. (1) with the two free parameters \mathcal{A}_s and n_s .

- We assume negligible contributions from tensor modes. In practice we set the tensor-to-scalar ratio r to zero (on this point see, however, Section V C).

To summarize, our Λ CDM model depends on the free parameters

$$\theta_{\Lambda\text{CDM}} = \{H_0, \Omega_{\text{cdm}}h^2, \Omega_{\text{b}}h^2, z_{\text{re}}, \mathcal{A}_{\text{s}}, n_{\text{s}}\}, \quad (12)$$

in addition to which one must include the PPS modification (2) with the choices (3), (5) or (8) for $\xi(k)$, thus extending the Λ CDM parameter space $\theta_{\Lambda\text{CDM}}$ by the additional $\theta_{\xi} = \{k_{\text{c}}, \lambda, \alpha, \beta\}$ (depending on the case at hand).

As our last ingredient we need the Planck Foreground and Instruments (PFI) parameters (available in Refs. [16, 17]), yielding a final extended parameter space

$$\theta = \theta_{\Lambda\text{CDM}} \cup \theta_{\xi} \cup \theta_{\text{PFI}}. \quad (13)$$

III. METHODOLOGY

In our analysis we employ three different CMB data sets (with the same nomenclature as in Ref. [17]). The likelihoods are split into low- ℓ (for $\ell \in (2, 29)$) and high- ℓ (for $\ell \geq 30$). The software adopted is the Planck likelihood code Plik-2.0 (as in Ref. [17]). Our three data sets are as follows:

- Planck TT : This refers to the low- ℓ and high- ℓ likelihoods for CMB temperature anisotropies only (that is, for C_{ℓ}^{TT} only). These two likelihoods are labeled by L_{low} and L_{high} respectively. The corresponding files for the likelihood code are:

- low- ℓ : commander_rc2_v1.1.l2.29.B.clik;
- high- ℓ : plik_dx11dr2_HM_v18_TT.clik;

- Planck TT +lowP: This includes the polarization data in addition to that of Planck TT for the low- ℓ section, specifically C_{ℓ}^{TE} , C_{ℓ}^{EE} and C_{ℓ}^{BB} for $\ell \in (2, 29)$. Note that we use the symbol L_{lowP} to refer to the combination of temperature and polarization for low multipoles. The corresponding files for the likelihood code are:

- low- ℓ :
lowl_SMW_70_dx11d_2014_10_03_v5c_Ap.clik;
- high- ℓ : plik_dx11dr2_HM_v18_TT.clik;

- Planck $TTTEEE$ +lowP: This includes, in addition to Planck TT +lowP, the polarization data C_{ℓ}^{TE} and C_{ℓ}^{EE} for the high- ℓ likelihood. We use the symbol L_{highP} to refer to this combination of temperature and polarization for high multipoles. The corresponding files for the likelihood code are:

- low- ℓ :
lowl_SMW_70_dx11d_2014_10_03_v5c_Ap.clik;

- high- ℓ : plik_dx11dr2_HM_v18_TTTEEE.clik;

Besides the above data likelihoods, the PFI prior is labeled by L_{PFI} (for simplicity we also use the symbol L here even though this is not a likelihood).

In addition to CMB data we also consider the 2.4% determination of the local value of the Hubble constant [18]. Here we use only their best estimate $H_0 = 73.24 \pm 1.74 \text{ km sec}^{-1} \text{ Mpc}^{-1}$, labeling it as H_0 and its likelihood as L_{H_0} . In our analysis we also include Baryonic Acoustic Oscillation data. We employ the detected BAO signals obtained from the large-scale correlation function determined with:

- galaxies from the 6dF Galaxy Survey (6dFGS) [19];
- galaxies with $z < 0.2$ from the Sloan Digital Sky Survey (SDSS) Data Release 7 (DR7) [20];
- galaxies from SDSS DR12 in the redshift interval $0.2 < z < 0.75$ [21];
- 147,000 quasars from the extended Baryon Oscillation Spectroscopic Survey (eBOSS) within $0.8 < z < 2.2$ [22];
- 137,562 quasars with redshifts $2.1 \leq z \leq 3.5$ from the DR11 of the BOSS/SDSS-III [23];
- cross-correlation of quasars with the Lyman alpha forest absorption, using over 164,000 quasars from DR11 of the BOSS/SDSS-III [24];

The combination of all BAO data is included in the likelihood L_{BAO} .

In this paper we are interested in answering the following question: assuming that the true PPS is given by $\mathcal{P}_{\text{F}}(k)$, what is the probability that an alternative PPS provides a better fit by pure chance? Our strategy is to calculate this probability considering the whole fit, even though the alternative PPS differs from the (assumed) true PPS mainly on large scales. We use the results of the full fit to study the model quality, including small scales and the other data sets. This avoids any kind of look-elsewhere effect and tackles the problem in a different way. There are many works in the recent literature modeling the large-scale behavior of the CMB anisotropies and trying to obtain a localized signature of a physical process (see for example Ref. [25] and references therein), whereas in our analysis we also study the compatibility of the modifications with other data sets (as well as their significance).

To discriminate quickly between our models, we first address the problem in a frequentist framework adopting the Likelihood-Ratio Test (LRT) [26, 27]. We apply this test by first identifying the full parameter space θ (see Eq. (13)), where each parametrization of $\xi(k)$ introduced in Sec. II satisfies

$$\lim_{k_{\text{c}} \rightarrow 0} \xi(k) = 1 \quad \Rightarrow \quad \lim_{k_{\text{c}} \rightarrow 0} \mathcal{P}(k) = \mathcal{P}_{\text{F}}(k).$$

(For the **atan** and **expc** models this also occurs for $\beta = 1$.) In other words, the fiducial model is nested in the parameter space θ . In the fitting process we use the parameter $q_c = \ln(k_c \times 1 \text{ Mpc})$ (that is numerically, in units of inverse Mpc) instead of k_c . This speeds up the numerical fitting process since the parameter k_c can vary by orders of magnitude in a fit. Furthermore, for any value² $q_c \ll \ln(H_0/c \times 1 \text{ Mpc})$ the deficit function $\xi(k)$ is close to one in the whole physical range of k that influences the CMB anisotropies and is therefore numerically indistinguishable from being taken as exactly one. Thus the fiducial model corresponds to any value of $q_c \ll \ln(H_0/c \times 1 \text{ Mpc})$. The Maximum Likelihood Estimator (MLE) for θ is given by

$$\hat{\theta} = \min_{\theta} \{-2 \ln [L(D|\theta)]\},$$

where D represents the data set to be used (in our case Planck TT , Planck TT +lowP or Planck $TTTEEE$ +lowP and their combinations with H0, BAO and H0+BAO), so that $L(D|\theta)$ is given by the appropriate product of

$$L_{\text{low}}, L_{\text{high}}, L_{\text{lowP}}, L_{\text{highP}}, L_{\text{PFI}}, L_{\text{H0}}, L_{\text{BAO}}.$$

On the other hand the MLE for the fiducial subspace is given by

$$\hat{\theta}_{\text{F}} = \min_{\theta_{\text{F}}} \{-2 \ln [L(D|\theta_{\text{F}})]\}, \quad \theta_{\text{F}} \equiv \theta_{\Lambda\text{CDM}} \cup \theta_{\text{PFI}}. \quad (14)$$

We then introduce the LRT statistic

$$\Gamma \equiv -2 \ln \left[\frac{L(D|\hat{\theta}_{\text{F}})}{L(D|\hat{\theta})} \right]. \quad (15)$$

It is easy to convince oneself that $\Gamma \geq 0$ since $L(D|\hat{\theta}) \geq L(D|\hat{\theta}_{\text{F}})$. To better understand the effects of ξ in each likelihood we also define the individual ratios

$$\Gamma_i \equiv -2 \ln \left[\frac{L_i(\hat{\theta}_{\text{F}})}{L_i(\hat{\theta})} \right], \quad (16)$$

where i denotes any of (low, lowP, high, highP, BAO, H0, PFI).

In principle if we know $P(\Gamma)$ – the probability distribution of Γ – then all we need is to find $\hat{\theta}_{\text{F}}$ and $\hat{\theta}$ in order to compute the probability of obtaining a better fit of D in θ by chance. This probability is simply given by

$$\gamma = \int_{\Gamma}^{\infty} d\Gamma' P(\Gamma'). \quad (17)$$

Note that we choose the right-hand tail since this corresponds to a $\hat{\theta}$ where the data is more probable than for

$\hat{\theta}_{\text{F}}$. In practice, unfortunately, $P(\Gamma)$ is not known and is hardly calculable as it would be impractical to obtain it from first principles given the complexity of the data likelihood. For this reason we must rely on Wilks' theorem, which asserts that in the large-sample limit Γ asymptotically follows a χ_r^2 distribution (for a proof see Ref. [28]), where r is the difference in dimensionality between θ and θ_{F} . Wilks' theorem requires the fiducial model to be contained within the parameter space. This is satisfied by the parameter q_c discussed above since the fiducial model requires only that $q_c \ll \ln(H_0/c \times 1 \text{ Mpc})$ and/or $\beta = 1$. In our parameterizations the largest dimension of $\xi(k)$ is 4. We list the critical value of Γ corresponding to a 2σ probability (that is, 95.45%) for the relevant cases:

$$\chi_1^2 = 4, \quad \chi_2^2 = 6.18, \quad \chi_3^2 = 8.02, \quad \chi_4^2 = 9.72. \quad (18)$$

In other words, with one extra parameter ($r = 1$) a fit giving $\Gamma > 4$ means that the fiducial model could only have generated a data set giving this value of Γ with a probability below 4.55%, and so on for more parameters.

It is worth noting that the LRT has some specific features which are of interest in our case. First, it does not depend on the choice of variables to describe the parameter space θ . Second, it naturally takes into account the difference in the number of parameters when comparing two nested models (see [28]). An important caveat when using the χ_r^2 distribution is that it relies on the asymptotic properties of the LRT.

Another aspect of the LRT worth mentioning is that it controls the type-I error, that is, cases where the fiducial model is true but is found to be false. For our choice of 2σ we would make a type-I error 4.55% of the time. However there is also the type-II error, that is, cases where the alternative model is true but is found to be false. Unlike for the type-I error, the LRT does not provide a simple way to calculate the probability of a type-II error. We could derive this probability analytically if the likelihood was sufficiently simple. But in practice the likelihood is too complicated and one must resort to simulations. A set of simulations of the alternative model must then be produced and, for each simulation, a value of $\{\Gamma_n\}$ must be calculated. Using this empirical distribution of Γ , one can then calculate the probability of a type-II error. In this work we do not address this point. But it is important to bear in mind the possibility that, if a very small critical region is required, one may be significantly increasing the type-II error. This would be the case, for example, if one were requiring 5σ instead of 2σ .

As is clear from the above discussion, the difference in the number of parameters between the fiducial and alternative models is crucial in determining the significance of the result (see Eq. (18)). Moreover, the use of a χ_r^2 distribution is based on the large-sample asymptotic limit. For this reason we note that, if a parameter controls a region of the model where there are almost no data, then we do not expect the asymptotic regime to be attained. For example, consider the parameter α discussed in Sec. II. It modifies the PPS only in a rather narrow band of k

² Here the speed of light c enters the numerical analysis (given the units used).

TABLE I. Fit and γ using Planck TT .

$\xi(k)$	$k_c^{-1}[\text{Gpc}]$	λ	β	α	h	n_s	$\ln(10^{10}\mathcal{A}_s)$	τ	Γ	Γ_{low}	Γ_{high}	γ
plaw	–	–	–	–	0.690	0.979	3.219	0.146	0.00	0.00	0.00	–
bpl	2.867	7.873	–	–	0.687	0.976	3.199	0.135	2.71	2.87	–0.04	25.76% (1.13 σ) [2]
atan1	3.587	1.000	0.000	1.000	0.696	0.975	3.303	0.185	5.50	4.36	1.00	1.90% (2.35 σ) [1]
atan2	1.436	1.000	0.489	1.000	0.703	0.971	3.370	0.216	5.82	5.23	0.44	5.45% (1.92 σ) [2]
atan3	1.683	1.000	0.471	0.935	0.699	0.971	3.344	0.203	5.91	5.05	0.70	11.59% (1.57 σ) [3]
atan4	0.357	41.294	0.793	0.577	0.690	0.978	3.254	0.163	6.93	6.26	0.57	13.95% (1.48 σ) [4]
expc1	2.094	0.500	0.000	–	0.694	0.979	3.286	0.180	5.61	4.70	0.80	1.78% (2.37 σ) [1]
expc2	2.687	0.439	0.000	–	0.692	0.977	3.276	0.174	5.84	4.91	0.83	5.40% (1.93 σ) [2]
expc3	0.334	14.068	0.782	–	0.691	0.979	3.273	0.173	6.73	6.17	0.43	8.12% (1.74 σ) [3]
jump	0.357	–	0.781	–	0.686	0.976	3.261	0.166	6.77	6.30	0.34	3.39% (2.12 σ) [2]

TABLE II. Fit and γ using Planck TT + H0.

$\xi(k)$	$k_c^{-1}[\text{Gpc}]$	λ	β	α	h	n_s	$\ln(10^{10}\mathcal{A}_s)$	τ	Γ	Γ_{low}	Γ_{high}	Γ_{H0}	γ
plaw	–	–	–	–	0.701	0.985	3.236	0.157	0.00	0.00	0.00	0.00	–
bpl	2.812	7.582	–	–	0.703	0.986	3.245	0.162	2.62	2.29	0.03	0.30	26.93% (1.10 σ) [2]
atan1	3.016	1.000	0.000	1.000	0.709	0.982	3.350	0.212	7.06	3.84	1.77	1.39	0.79% (2.66 σ) [1]
atan2	1.326	1.000	0.504	1.000	0.712	0.975	3.391	0.227	8.27	4.76	1.59	1.82	1.60% (2.41 σ) [2]
atan3	1.327	1.000	0.505	1.000	0.712	0.975	3.391	0.227	8.25	4.76	1.57	1.82	4.12% (2.04 σ) [3]
atan4	1.298	1.006	0.506	0.987	0.712	0.975	3.391	0.227	8.31	4.75	1.64	1.81	8.09% (1.75 σ) [4]
expc1	1.465	0.500	0.000	–	0.710	0.987	3.366	0.223	6.93	4.31	1.01	1.54	0.85% (2.63 σ) [1]
expc2	1.624	0.360	0.000	–	0.716	0.977	3.410	0.241	8.55	4.80	1.39	2.25	1.39% (2.46 σ) [2]
expc3	1.606	0.362	0.007	–	0.716	0.978	3.410	0.241	8.56	4.80	1.40	2.25	3.57% (2.10 σ) [3]
jump	0.353	–	0.763	–	0.704	0.988	3.326	0.203	7.17	5.87	0.76	0.57	2.77% (2.20 σ) [2]

TABLE III. Fit and γ using Planck TT + BAO.

$\xi(k)$	$k_c^{-1}[\text{Gpc}]$	λ	β	α	h	n_s	$\ln(10^{10}\mathcal{A}_s)$	τ	Γ	Γ_{low}	Γ_{high}	Γ_{BAO}	γ
plaw	–	–	–	–	0.684	0.975	3.205	0.137	0.00	0.00	0.00	0.00	–
bpl	2.803	7.961	–	–	0.684	0.975	3.196	0.133	2.64	2.82	–0.13	–0.01	26.76% (1.11 σ) [2]
atan1	3.458	1.000	0.000	1.000	0.687	0.970	3.301	0.182	4.57	4.14	0.41	–0.18	3.25% (2.14 σ) [1]
atan2	1.981	1.000	0.477	1.000	0.688	0.964	3.305	0.181	5.02	5.01	0.09	–0.18	8.12% (1.74 σ) [2]
atan3	1.981	1.000	0.477	1.000	0.688	0.964	3.305	0.181	5.02	5.01	0.09	–0.18	17.02% (1.37 σ) [3]
atan4	0.350	48.232	0.768	0.506	0.690	0.979	3.294	0.183	5.45	6.53	–0.16	–1.07	24.40% (1.16 σ) [4]
expc1	2.232	0.500	0.000	–	0.685	0.974	3.260	0.164	5.30	4.66	0.52	–0.02	2.14% (2.30 σ) [1]
expc2	2.532	0.448	0.000	–	0.685	0.972	3.261	0.165	5.50	4.93	0.46	0.02	6.40% (1.85 σ) [2]
expc3	0.333	19.941	0.787	–	0.685	0.975	3.254	0.162	6.68	6.38	0.14	–0.02	8.28% (1.73 σ) [3]
jump	0.361	–	0.790	–	0.684	0.975	3.252	0.161	6.76	6.38	0.22	0.03	3.40% (2.12 σ) [2]

TABLE IV. Fit and γ using Planck TT + H0 + BAO.

$\xi(k)$	$k_c^{-1}[\text{Gpc}]$	λ	β	α	h	n_s	$\ln(10^{10}\mathcal{A}_s)$	τ	Γ	Γ_{low}	Γ_{high}	Γ_{H0}	Γ_{BAO}	γ
plaw	–	–	–	–	0.688	0.977	3.191	0.131	0.00	0.00	0.00	0.00	0.00	–
bpl	2.960	7.919	–	–	0.689	0.977	3.201	0.136	2.60	2.18	0.34	0.08	–0.05	27.23% (1.10 σ) [2]
atan1	3.896	1.000	0.000	1.000	0.691	0.972	3.279	0.172	5.57	3.52	1.61	0.80	–0.53	1.82% (2.36 σ) [1]
atan2	2.579	1.000	0.486	1.000	0.692	0.969	3.279	0.171	5.75	4.03	1.28	0.94	–0.62	5.64% (1.91 σ) [2]
atan3	1.442	1.000	0.502	0.544	0.691	0.969	3.278	0.171	5.78	4.01	1.39	0.79	–0.50	12.29% (1.54 σ) [3]
atan4	0.348	45.708	0.766	0.524	0.691	0.979	3.295	0.184	6.54	5.58	0.58	0.63	–0.46	16.24% (1.40 σ) [4]
expc1	2.106	0.500	0.000	–	0.691	0.977	3.282	0.177	5.75	3.81	1.41	0.63	–0.37	1.65% (2.40 σ) [1]
expc2	2.498	0.439	0.000	–	0.690	0.976	3.281	0.176	6.03	4.13	1.35	0.48	–0.20	4.91% (1.97 σ) [2]
expc3	0.332	17.363	0.768	–	0.690	0.979	3.289	0.181	6.55	5.46	0.70	0.55	–0.38	8.76% (1.71 σ) [3]
jump	0.354	–	0.769	–	0.690	0.979	3.287	0.180	6.70	5.56	0.76	0.31	–0.14	3.50% (2.11 σ) [2]

around k_c , and it also modifies the PPS only slightly at this point. Consequently, we expect this parameter to be very degenerate and not to contribute much to the fit. In an extreme case where the alternative model has a parameter that does not modify the PPS fit at all, it is reasonable to assume that the current data are not able to shed any light on that aspect of the model. In such a case we also perform the statistical tests with the degenerate parameter removed from the analysis (keeping it fixed at some fiducial value), and we do not take that parameter into account when comparing the alternative and fiducial models. This ambiguity in the number of parameters is a natural feature of our phenomenological approach. Thus the two relevant questions are: what kind of modification of the fiducial model is the data able to fit, and what is the significance of this fit?

The standard Bayesian approach in this case uses the Bayes factor

$$B_{\text{FA}} = \frac{\int d\theta L(D|\hat{\theta})P(\theta)}{\int d\theta_{\text{F}} L(D|\hat{\theta}_{\text{F}})P_{\text{F}}(\theta_{\text{F}})}, \quad (19)$$

where P_{F} and P are the respective priors in the fiducial and alternative models. As in Ref. [14], if we consider the same flat prior for both models ($P_{\text{F}}(\theta_{\text{F}}) = 1$ and $P(\theta) = 1$, besides the PFI priors cited above), the LRT gives us a point estimate of the Bayes factor:

$$B_{\text{FA}} \approx \exp\left(\frac{\Gamma}{2}\right).$$

In this work we do not initially follow the Bayesian approach for all the models for two reasons. First, as we stated above, in this phenomenological study we want to understand the ability of the current data to inform us about different aspects of the model, whereas a Bayesian approach would simply tend to penalize any irrelevant extra parameters in the alternative model. Our initial interest is in determining if those extra parameters should be included in the analysis. The second reason why we initially perform a frequentist analysis stems, again, from the phenomenological nature of our approach: we may not have any theoretical reason to assume a specific prior for the extra parameters, and in fact even a flat prior would not be unambiguous since it depends on the choice of parameters. Note that the frequentist approach does not depend on the introduction of a measure in the model space (usually done through simple priors in the model parameters).

A frequentist approach does not answer the same questions as a Bayesian methodology. All we can know in a frequentist study is the ability of the current data to falsify the fiducial model (the null hypothesis). In other words, if an alternative model provides a better fit to the data – one that goes beyond the improvement expected from statistical fluctuations and from the addition of extra parameters – then we may say that the fiducial model

is falsified.³ Since we will be evaluating a large number of cases we choose first to follow the frequentist approach, thereby answering the simplest questions while avoiding the introduction of an arbitrary and subjective measure in the model space. We then apply a follow-up Bayesian analysis to what appears to be the best competing model.

In our Bayesian approach we run a complete Markov Chain Monte Carlo (MCMC) analysis of the posteriors of the fiducial and competing models using an ensemble sampler algorithm that was introduced in Ref. [29]⁴ and which is here implemented in NumCosmo as described in App. A. From the results we produce a corner plot containing the marginal distributions and two-dimensional confidence regions for all relevant parameters. We then apply the modified harmonic mean, also described in App. A, to estimate the Bayes factor resulting from the comparison of the fiducial and competing models.

IV. NUMERICAL APPROACH

The theoretical CMB anisotropies C_{ℓ}^{XY} do not depend on the Planck foreground and instrument parameters in θ_{PFI} . For this reason we divide the problem of finding the best fit into two steps. In the first step, we define the full Planck likelihood $L(D|\theta)$ as a function on the whole parameter space. Fixing the values of $\{\theta_{\Lambda\text{CDM}}, \theta_{\xi}\}$, we can cheaply calculate the likelihood for different points of θ_{PFI} since we can re-use the same C_{ℓ}^{XY} . We then define the PFI-Likelihood as

$$L_{\text{PFI}}(D|\theta_{\Lambda\text{CDM}}, \theta_{\xi}) = \max_{\theta_{\text{PFI}}} L(D|\theta). \quad (20)$$

In the second step, we find the maximum of $L_{\text{PFI}}(D|\theta_{\Lambda\text{CDM}}, \theta_{\xi})$. Even though these two steps are mathematically equivalent (when the Likelihood is smooth), numerically they speed up the finding of the best fit significantly. In App. A we describe the specific objects and methods used at this stage.

For the computation of C_{ℓ}^{XY} we employ the CLASS back end of NumCosmo (see Refs. [31–33]). Since in this case we are measuring differences in the PPS, we use three different precision configurations: Low Precision (LP) (the default to CLASS, as in their version 2.5.0), Medium Precision (MP), and High Precision (HP). The results with LP and MP differ significantly, whereas the results with MP and HP are essentially the same. For this reason, in what follows we report only the MP results.

³ Of course, to obtain the relevant probabilities it is necessary to simulate a large number of samples from the fiducial and alternative models, or to use Wilks' theorem which only includes the probability of the data under the null hypothesis.

⁴ There also exists a Python implementation, see Ref. [30].

TABLE V. Fit and γ using Planck TT + lowP.

$\xi(k)$	$k_c^{-1}[\text{Gpc}]$	λ	β	α	h	n_s	$\ln(10^{10}\mathcal{A}_s)$	τ	Γ	Γ_{low}	Γ_{high}	γ
plaw	–	–	–	–	0.676	0.968	3.104	0.085	0.00	0.00	0.00	–
bpl	1.158	0.678	–	–	0.679	0.969	3.132	0.100	2.15	0.90	1.06	34.16% (0.95 σ) [2]
atan1	5.269	1.000	0.000	1.000	0.678	0.963	3.151	0.106	3.47	2.33	1.08	6.25% (1.86 σ) [1]
atan2	5.194	1.000	0.010	1.000	0.676	0.962	3.150	0.105	3.52	2.39	1.09	17.20% (1.37 σ) [2]
atan3	3.659	1.000	0.009	0.515	0.676	0.963	3.149	0.105	3.64	2.14	1.43	30.30% (1.03 σ) [3]
atan4	0.376	37.218	0.805	0.511	0.676	0.967	3.147	0.106	5.02	3.00	1.87	28.56% (1.07 σ) [4]
expc1	2.894	0.500	0.000	–	0.676	0.966	3.156	0.110	3.85	1.79	1.86	4.99% (1.96 σ) [1]
expc2	2.700	0.515	0.000	–	0.676	0.966	3.155	0.110	3.87	1.84	1.82	14.44% (1.46 σ) [2]
expc3	0.353	13.593	0.799	–	0.676	0.967	3.154	0.109	4.71	2.52	1.95	19.42% (1.30 σ) [3]
jump	0.372	–	0.811	–	0.676	0.967	3.145	0.105	5.06	3.12	1.68	7.97% (1.75 σ) [2]

TABLE VI. Fit and γ using Planck TT + lowP + H0.

$\xi(k)$	$k_c^{-1}[\text{Gpc}]$	λ	β	α	h	n_s	$\ln(10^{10}\mathcal{A}_s)$	τ	Γ	Γ_{lowP}	Γ_{high}	Γ_{H0}	γ
plaw	–	–	–	–	0.689	0.974	3.114	0.093	0.00	0.00	0.00	0.00	–
bpl	1.173	0.714	–	–	0.692	0.977	3.142	0.107	2.93	1.02	0.85	0.89	23.11% (1.20 σ) [2]
atan1	5.609	1.000	0.000	1.000	0.691	0.970	3.160	0.114	3.80	1.60	1.60	0.49	5.12% (1.95 σ) [1]
atan2	5.438	1.000	0.007	1.000	0.691	0.970	3.160	0.114	3.85	1.62	1.78	0.38	14.57% (1.46 σ) [2]
atan3	3.560	1.000	0.003	0.501	0.691	0.972	3.168	0.118	4.14	1.00	2.40	0.50	24.62% (1.16 σ) [3]
atan4	0.379	40.773	0.813	0.564	0.687	0.973	3.153	0.111	4.69	2.01	3.16	–0.68	32.01% (0.99 σ) [4]
expc1	3.237	0.500	0.000	–	0.690	0.974	3.161	0.116	3.99	1.13	2.27	0.30	4.58% (2.00 σ) [1]
expc2	2.722	0.569	0.000	–	0.691	0.975	3.159	0.116	4.07	1.08	2.33	0.41	13.05% (1.51 σ) [2]
expc3	0.360	14.399	0.809	–	0.688	0.974	3.166	0.118	4.53	1.01	3.64	–0.44	20.97% (1.25 σ) [3]
jump	0.374	–	0.813	–	0.690	0.975	3.166	0.119	4.61	1.02	2.93	0.30	9.99% (1.65 σ) [2]

TABLE VII. Fit and γ using Planck TT + lowP + BAO.

$\xi(k)$	$k_c^{-1}[\text{Gpc}]$	λ	β	α	h	n_s	$\ln(10^{10}\mathcal{A}_s)$	τ	Γ	Γ_{lowP}	Γ_{high}	Γ_{BAO}	γ
plaw	–	–	–	–	0.680	0.970	3.108	0.088	0.00	0.00	0.00	0.00	–
bpl	1.187	0.627	–	–	0.681	0.970	3.124	0.096	2.32	1.24	1.06	0.06	31.40% (1.01 σ) [2]
atan1	5.274	1.000	0.000	1.000	0.681	0.965	3.160	0.112	3.54	1.76	1.70	0.08	6.01% (1.88 σ) [1]
atan2	5.274	1.000	0.000	1.000	0.681	0.965	3.160	0.112	3.54	1.76	1.70	0.08	17.07% (1.37 σ) [2]
atan3	5.274	1.000	0.000	1.000	0.681	0.965	3.160	0.112	3.54	1.76	1.70	0.08	31.62% (1.00 σ) [3]
atan4	0.371	45.702	0.816	0.520	0.682	0.971	3.154	0.110	4.57	2.42	1.94	0.14	33.45% (0.97 σ) [4]
expc1	2.974	0.500	0.000	–	0.681	0.969	3.158	0.113	3.84	1.63	2.00	0.05	5.00% (1.96 σ) [1]
expc2	2.974	0.527	0.000	–	0.681	0.969	3.145	0.107	3.88	2.09	1.64	0.08	14.40% (1.46 σ) [2]
expc3	0.353	17.005	0.804	–	0.681	0.970	3.165	0.116	4.37	1.64	2.37	0.10	22.42% (1.22 σ) [3]
jump	0.370	–	0.798	–	0.682	0.971	3.170	0.119	4.35	1.37	2.60	0.11	11.37% (1.58 σ) [2]

TABLE VIII. Fit and γ using Planck TT + lowP + H0 + BAO.

$\xi(k)$	$k_c^{-1}[\text{Gpc}]$	λ	β	α	h	n_s	$\ln(10^{10}\mathcal{A}_s)$	τ	Γ	Γ_{lowP}	Γ_{high}	Γ_{H0}	Γ_{BAO}	γ
plaw	–	–	–	–	0.685	0.972	3.127	0.098	0.00	0.00	0.00	0.00	0.00	–
bpl	1.164	0.694	–	–	0.686	0.973	3.134	0.102	2.85	2.47	0.14	0.34	–0.12	24.04% (1.17 σ) [2]
atan1	5.719	1.000	0.000	1.000	0.685	0.967	3.146	0.105	3.87	3.82	0.02	0.17	0.01	4.92% (1.97 σ) [1]
atan2	5.720	1.000	0.000	1.000	0.685	0.967	3.146	0.105	3.87	3.82	0.02	0.17	0.01	14.41% (1.46 σ) [2]
atan3	5.719	1.000	0.000	1.000	0.685	0.967	3.146	0.105	3.88	3.82	0.03	0.17	0.01	27.48% (1.09 σ) [3]
atan4	0.375	42.398	0.820	0.521	0.686	0.972	3.153	0.111	4.95	3.52	1.10	0.43	–0.15	29.28% (1.05 σ) [4]
expc1	3.074	0.500	0.000	–	0.685	0.971	3.156	0.113	4.22	2.88	1.13	0.17	0.00	4.00% (2.05 σ) [1]
expc2	3.074	0.500	0.000	–	0.685	0.971	3.156	0.113	4.22	2.88	1.13	0.17	0.00	12.13% (1.55 σ) [2]
expc3	0.356	15.636	0.805	–	0.686	0.972	3.165	0.117	4.72	2.63	1.68	0.30	–0.05	19.34% (1.30 σ) [3]
jump	0.373	–	0.807	–	0.686	0.973	3.169	0.119	4.76	2.46	1.83	0.30	–0.04	9.24% (1.68 σ) [2]

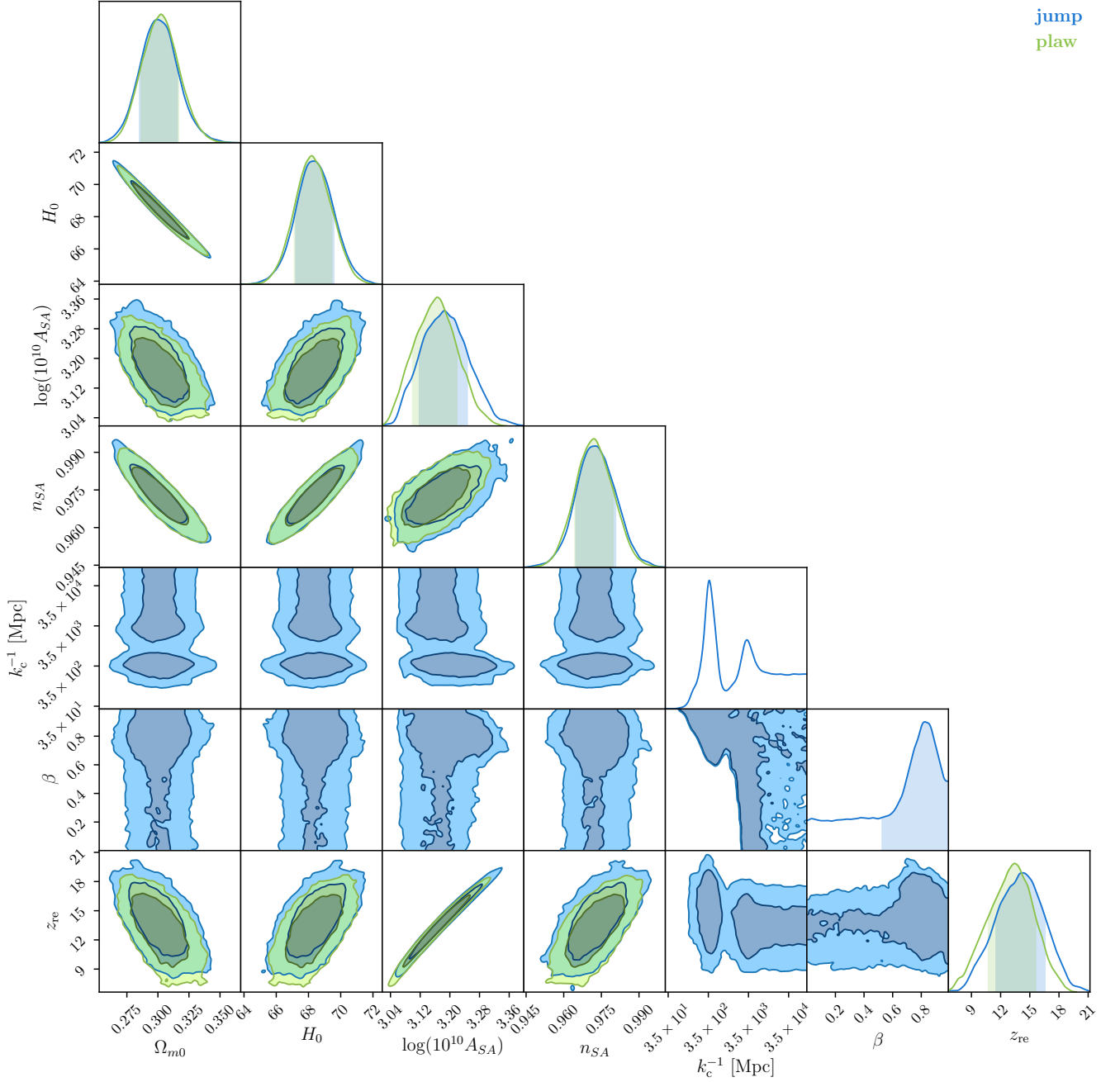


FIG. 2. Corner plot for the MCMC results with **plaw** and **jump** using Planck TT . The marginal distribution for k_c^{-1} has two modes, the first at 378 Mpc and the second at 3291 Mpc. As expected the distribution for k_c^{-1} becomes flat for $k_c^{-1} > 3291$ Mpc, since at these values the **jump** mode is numerically equivalent to **plaw**. Furthermore, in this interval, the distribution for β becomes completely degenerate as can be seen in the $k_c^{-1} \times \beta$ confidence region. This is the reason why the short distance mode appears to provide a definite set of values and may therefore be considered physically relevant, while the second, long distance mode, is too degenerate in the actual value of the jump's amplitude, not to mention that the scale induced is very close to the Hubble scale; we thus do not consider this mode any further.

V. RESULTS

We group our results according to which CMB data we are using. For a given CMB sample we discuss its results alone and in combination with the other samples H0, BAO and H0+BAO. We already know from previous studies (see for example [14] and references therein) that there is a lack of power on large scales for the temperature data. However, studying this effect alone can be misleading as it is difficult to take into account the look-elsewhere effect when we are dealing with a large and heterogeneous body of data. We therefore compare the whole fit when using different data sets, and we also include the differences in the fit for each relevant part of the likelihood.

A. General considerations

We summarize our results in Tables I to XII. For each parameterization and data set used, we show the best-fit values of the cut-off scale k_c^{-1} in Gpc and (when relevant) the values of the dimensionless parameters λ , β and α . The first (λ) measures the sharpness of the deficit function, the second (β) quantifies the deficit, while the third (α) describes the shape of the transition. After these four new parameters we include the best-fit values of the four standard parameters: the dimensionless rescaled Hubble scale h , the spectral index n_s and amplitude A_s of the fiducial PPS (1), and finally the reionization optical depth τ . To complete the tables we add the LRT statistics Γ defined by (15) and (in the last column) the p -value γ defined by (17). To the last column we add (in round brackets) the probability γ translated into the corresponding number of one-dimensional Gaussian standard deviations, and also (in square brackets) the number of extra degrees of freedom. It is often assumed that a p -value of 5% indicates statistical significance. We shall here instead take the view that whenever a small value is found, this merely suggests a plausible new effect.

In the first line of Table IX we reproduce the currently accepted values for the four standard-model parameters h , n_s , A_s and τ , where our fit matches that provided by the Planck team (see, however, App A).

The first conclusion one can draw from these tables is that the standard-model parameters are hardly affected by the inclusion of the deficit function, regardless of the choice of the latter. This shows that even if the lack of power is a true physical phenomenon, it cannot come from a strong effect as otherwise the analysis would have shown some instability when including this phenomenon in the description of the data. This also immediately shows that there is no chance, as might have been hoped, of resolving the H_0 tension by taking the deficit function into account. Indeed, the closest we get to resolving the tension is revealed in Tab. II, where we see that a reasonable amount of the significance is produced by a better fitting of the H0 data (see Γ_{H0}). However, this effect is

severely reduced when polarization data are added. In other words, when fitting TT data alone the extra freedom in the PPS seems to allow a better fit of the $TT + H0$ data combination, but this does not hold when polarization data are added. On the contrary, comparing with the **plaw** fits including H0, we see that when polarization data (at both low- ℓ and high- ℓ) are added we get $-2\ln(L_{H0}) \approx 9$, which corresponds roughly to the well-known 3σ tension with the H0 data. For this reason, our results including H0 should be interpreted with caution.

The fit of the fiducial spectrum is remarkably stable, with n_s and A_s varying (all over the range of our analysis) by less than 3% and 10% respectively compared with their fiducial values. It should also be noted that these extreme values are obtained using the TT data only together with the H0 set.

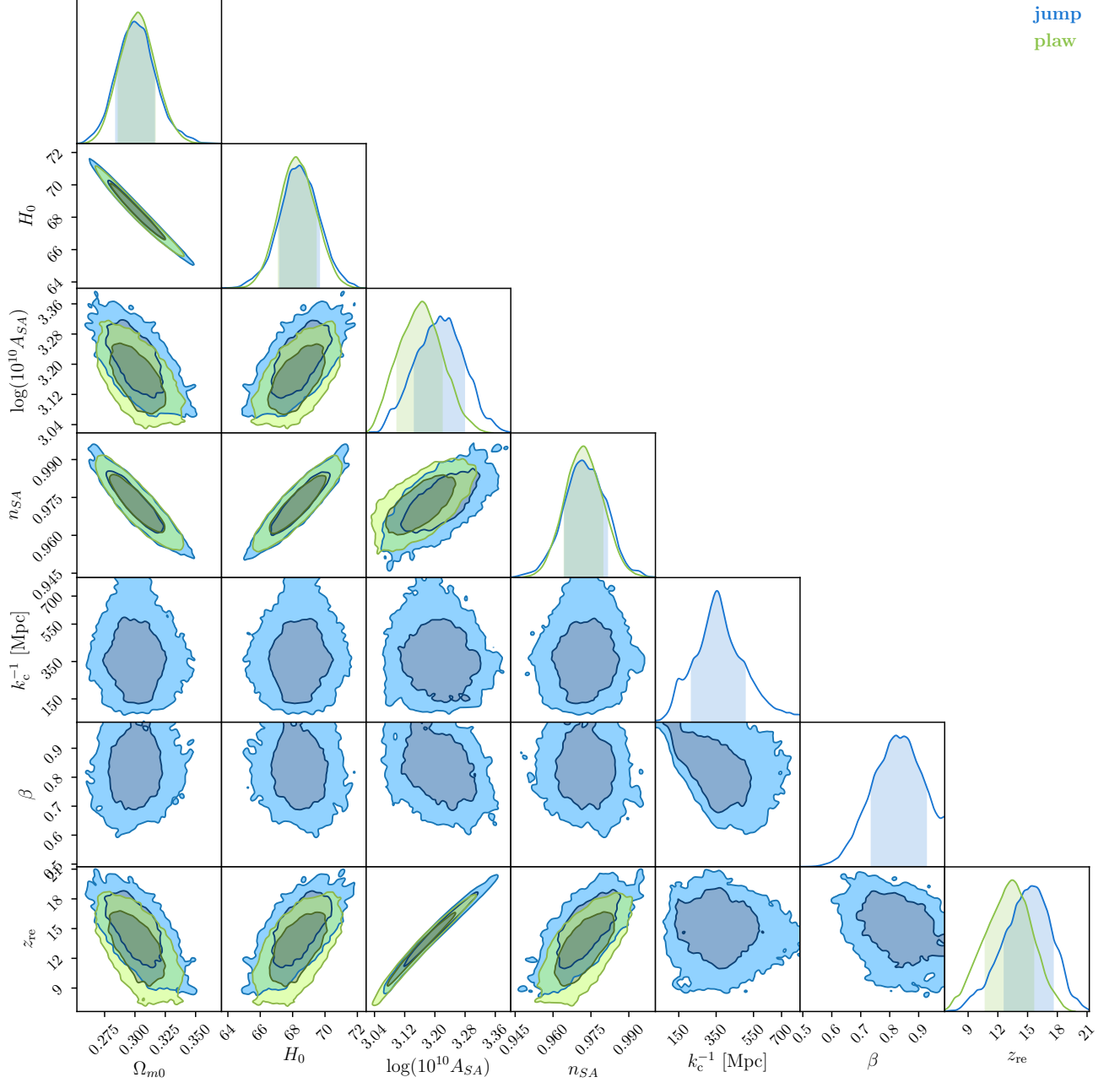
Finally, the reionization optical depth τ is the parameter subject to the highest variation in our analysis. Even with only the TT data together with the H0 set, we find that τ can change by a large factor. This is a general trend with the other data sets too, as can be checked explicitly in the tables, with a variation by a factor of up to almost 3.

B. The deficit function

Throughout the data, if we set the interval for the parameter λ to be around unity⁵ (that is, if we impose a smooth transition), it is found that the best-fit value of the transition scale remains very close to the Hubble radius – where the data are variance-dominated. As a result, these fits are only marginally significant (like those originally discussed by the Planck team). Adding data for polarization, H0 and the BAOs does not change this trend, and in fact adding polarization actually reduces the significance.

Our weakly-significant fits neither support nor rule out the smooth deficit functions we have studied. Statistically speaking, according to our frequentist analysis, these functions are more or less as successful as the standard power-law model (taking into account the larger number of parameters). This result might be viewed as a modest success, in the sense that a smooth deficit could have been disfavored compared to no deficit but instead performs comparably well. On the other hand, the data we have studied are consistent with the apparent low power being a mere statistical fluctuation. In the absence of a significantly better fit for the models with a smooth deficit, it is also natural to invoke Ockham's razor to favor the simpler model with no extra parameters (even

⁵ This is not to be considered a prior as it is only a feature of the minimization algorithm. If in any event the minimization process takes the best-fit close to the boundaries of these intervals, then they should be extended and the minimization rerun.



jump
plaw

FIG. 3. Corner plot for the MCMC results from **plaw** and **jump** using Planck TT after removing the second mode $k_c^{-1} = 3291\text{Mpc}$. In this plot we use a linear scale for k_c^{-1} . Note that once the second mode is removed, there is a shift in A_{SA} and z_{re} . This was already present in Fig 2, in the $k_c^{-1} \times \log(10^{10} A_{SA})$ and $k_c^{-1} \times z_{re}$ confidence regions, where the one-sigma contour related to the second mode of k_c^{-1} is slightly shifted when compared to the first mode. In addition, we have a negative correlation for $k_c^{-1} \times \beta$: a smaller jump scale k_c^{-1} implies a smaller jump amplitude (β gets closer to unity).

if, strictly speaking, no such conclusion can be drawn on the basis of the significance of the fits).

Furthermore, the data we have studied certainly cannot constrain the shape of the smooth-deficit spectrum even if it exists. This seems to be so regardless of the functional form of the deficit function (**exp**, **bpl** or **atan**), and independently of the number of extra parameters and priors assumed. This conclusion is compatible with our result that the shape parameter α is essentially irrelevant. Roughly speaking, we found α ranging between $\frac{1}{2}$ and 1. As shown in Fig. 1, this amounts to hardly any variation at all in the actual spectrum. Thus it appears that the data cannot favor any particular shape.

If we adopt the quantum relaxation deficit function (8) with the sharpness parameter λ freely varying (as was originally suggested in the Planck papers [13, 14] for the exponential cut-off and broken power-law deficit functions), we are led to a remarkable development in the fitting procedure. Our starting interval for λ was taken to be of order unity, which implies as we have mentioned a smooth transition around the Hubble scale. However, we found that the best-fit process consistently tried to reach the upper bound of the allowed interval for λ . Extending the upper bound on λ , we found the fit spontaneously pointing towards larger and larger values – that is, towards a sharper and sharper transition. This phenomenon suggested that we consider a very large interval for λ (with the full four-parameter space **atan4**). Finally, however, because a very large λ corresponds to a very sharp transition, we were led to re-analyze the data afresh with a new and simpler two-parameter sharp-deficit function:

$$\xi_{\text{jump}}(k) = \begin{cases} \beta & \text{for } k \leq k_c, \\ 1 & \text{for } k \geq k_c. \end{cases} \quad (21)$$

This is the deficit function employed in the tables under the label **jump**. It has some remarkable properties which we discuss in Sec. VII below.

C. Tensor modes and scalar-tensor consistency

In our data analysis we have ignored tensor modes (effectively assuming a negligible tensor-to-scalar ratio $r \simeq 0$). It is however noteworthy that, for both **atan** and **exp** as well as for **jump**, we have found a general degradation of the frequentist significance when polarization data are added (though noting that the parameters remain remarkably stable for **jump**). The pattern of degradation depends on the data sets considered. For example, comparing TT only (Table I) with the full Planck data (Table IX) the degradation of p -values for **atan** is worse than for **jump**, while comparing $TT + \text{BAO}$ (Table III) with $TT + \text{BAO} + \text{lowP}$ (Table VII) the degradation is worse for **jump**. For $TT + \text{BAO}$ and full Planck + BAO (Table XI) the degradations are comparable. On the other hand it should be noted that the Γ values are

persistently higher for **jump**, indicating that the degradation is less severe. To explain these observations, we may consider three possible scenarios.

First, we may imagine that we are in fact simply modeling a statistical fluke. This would imply that the more data we add, the smaller the resulting significance. However, this does not generally appear to be the case. Although there seems to be a systematic degradation when we add polarization data, adding other data sets does not result in any particular systematic (positive or negative) trend for the fits.

A second possibility is that our models are indeed fitting a real feature but also partially over-fitting some noise. In this case, adding more data may be expected to wash out the over-fit simply by reducing the noise, and this in turn would reduce the significance to its genuine value. For each of our deficit functions it can then happen that, because of an over-fitting of noise for data sets without polarization, significance is lost when polarization data are added. If this turns out to be the true explanation for the observed degradation, then **jump** will arguably be the preferred deficit function because of its persistently high values of Γ (though in terms of p -values it is not clear which function would be preferred).

The third scenario, which we focus on in this section, is related to the assumption of negligible tensor contributions. This is arguably something of a theoretical prejudice, stemming from the $\Lambda\text{CDM} + \text{inflation}$ paradigm with a small value of r (specifically $r_{0.002} < 0.099$, with 95% CL from temperature and polarization data), the relevant constraint being calculated within that framework. In contrast with this paradigmatic case, Ref [34] fitted several variants. For instance, allowing the possibility of a running spectral index for the scalar PPS, the upper bound on r becomes $r_{0.002} < 0.15$ (95% CL, with temperature and polarization data). Thus changing the framework (for example allowing for a running spectral index) permits us to relax the constraint on r . Including a deficit function in the PPS can be even more drastic as it can break scalar-tensor consistency. In the context of our analysis it is therefore natural to expect that a larger tensor contribution is allowed. We are then led to consider that the addition of a tensor contribution, with a breaking of scalar-tensor consistency, might enable us to avoid the degradation noted above. If this turns out to be the true explanation for the observed degradation, then **atan** will arguably be the preferred deficit function because (as discussed below) quantum relaxation models naturally allow for a breaking of scalar-tensor consistency.

The TT angular power spectra are functionals of the scalar (\mathcal{P}_S) and tensor (\mathcal{P}_T) power spectra:

$$C_\ell^{TT} = C_{S,\ell}^{TT}[\mathcal{P}_S] + C_{T,\ell}^{TT}[\mathcal{P}_T]. \quad (22)$$

We may parameterize \mathcal{P}_T with an amplitude $\mathcal{A}_T = r\mathcal{A}_S$ and write $\mathcal{P}_S = \mathcal{A}_S f(k)$ and $\mathcal{P}_T = r\mathcal{A}_S g(k)$. Since the functionals are linear we have

$$C_\ell^{TT} = A_S C_{S,\ell}^{TT}[f] + r A_S C_{T,\ell}^{TT}[g]. \quad (23)$$

TABLE IX. Fit and γ using Planck TT , TE , EE + lowP.

$\xi(k)$	$k_c^{-1}[\text{Gpc}]$	λ	β	α	h	n_s	$\ln(10^{10}\mathcal{A}_s)$	τ	Γ	Γ_{lowP}	Γ_{highP}	γ
plaw	–	–	–	–	0.673	0.966	3.100	0.082	0.00	0.00	0.00	–
bpl	0.215	0.137	–	–	0.674	0.965	3.139	0.101	4.69	2.65	1.89	9.56% (1.67 σ) [2]
atan1	6.491	1.000	0.000	1.000	0.673	0.960	3.129	0.094	3.36	2.83	0.65	6.69% (1.83 σ) [1]
atan2	6.455	1.000	0.000	1.000	0.673	0.960	3.128	0.094	3.36	2.83	0.82	18.65% (1.32 σ) [2]
atan3	6.540	1.000	0.003	0.980	0.673	0.960	3.129	0.094	3.36	2.77	0.76	33.93% (0.96 σ) [3]
atan4	0.375	31.287	0.824	0.699	0.672	0.964	3.120	0.091	5.73	4.31	1.29	22.03% (1.23 σ) [4]
expc1	3.390	0.500	0.000	–	0.673	0.965	3.138	0.100	4.04	2.41	1.60	4.45% (2.01 σ) [1]
expc2	2.742	0.574	0.000	–	0.674	0.965	3.134	0.099	4.16	2.29	1.80	12.51% (1.53 σ) [2]
expc3	0.349	13.077	0.817	–	0.673	0.965	3.130	0.096	5.70	3.83	1.73	12.72% (1.53 σ) [3]
jump	0.380	–	0.816	–	0.673	0.964	3.122	0.093	5.79	4.19	1.52	5.53% (1.92 σ) [2]

TABLE X. Fit and γ using Planck TT , TE , EE + lowP + H0.

$\xi(k)$	$k_c^{-1}[\text{Gpc}]$	λ	β	α	h	n_s	$\ln(10^{10}\mathcal{A}_s)$	τ	Γ	Γ_{lowP}	Γ_{highP}	Γ_{H0}	γ
plaw	–	–	–	–	0.680	0.970	3.111	0.089	0.00	0.00	0.00	0.00	–
bpl	0.223	0.142	–	–	0.680	0.969	3.144	0.105	4.78	2.55	2.07	–0.01	9.17% (1.69 σ) [2]
atan1	7.297	1.000	0.000	1.000	0.680	0.965	3.130	0.096	3.19	3.05	0.33	0.01	7.39% (1.79 σ) [1]
atan2	6.835	1.000	0.022	1.000	0.680	0.964	3.134	0.098	3.25	2.87	0.66	–0.11	19.73% (1.29 σ) [2]
atan3	4.823	1.000	0.005	0.511	0.680	0.965	3.123	0.094	3.28	3.20	0.23	0.02	35.00% (0.93 σ) [3]
atan4	0.391	31.476	0.821	0.765	0.680	0.968	3.131	0.099	5.49	3.74	1.63	–0.06	24.10% (1.17 σ) [4]
expc1	3.671	0.500	0.000	–	0.680	0.969	3.141	0.104	4.13	2.41	1.57	0.08	4.21% (2.03 σ) [1]
expc2	2.824	0.582	0.000	–	0.681	0.969	3.139	0.103	4.16	2.27	1.60	0.20	12.48% (1.53 σ) [2]
expc3	0.357	13.664	0.819	–	0.679	0.968	3.140	0.103	5.46	3.34	2.23	–0.32	14.12% (1.47 σ) [3]
jump	0.385	–	0.825	–	0.680	0.968	3.124	0.095	5.30	4.11	0.99	0.08	7.07% (1.81 σ) [2]

TABLE XI. Fit and γ using Planck TT , TE , EE + lowP + BAO.

$\xi(k)$	$k_c^{-1}[\text{Gpc}]$	λ	β	α	h	n_s	$\ln(10^{10}\mathcal{A}_s)$	τ	Γ	Γ_{lowP}	Γ_{highP}	Γ_{BAO}	γ
plaw	–	–	–	–	0.678	0.968	3.105	0.085	0.00	0.00	0.00	0.00	–
bpl	0.234	0.144	–	–	0.678	0.968	3.143	0.104	4.74	2.32	2.21	–0.03	9.36% (1.68 σ) [2]
atan1	7.007	1.000	0.000	1.000	0.678	0.964	3.128	0.095	3.19	2.94	0.59	–0.08	7.39% (1.79 σ) [1]
atan2	6.972	1.000	0.013	1.000	0.678	0.964	3.133	0.097	3.24	2.69	0.73	–0.15	19.80% (1.29 σ) [2]
atan3	4.446	1.000	0.002	0.508	0.677	0.964	3.125	0.094	3.43	2.96	0.86	–0.25	33.03% (0.97 σ) [3]
atan4	0.371	31.684	0.820	0.675	0.678	0.968	3.135	0.101	5.53	3.54	1.92	–0.06	23.68% (1.18 σ) [4]
expc1	3.503	0.500	0.000	–	0.677	0.967	3.139	0.102	4.10	2.37	2.00	–0.28	4.28% (2.03 σ) [1]
expc2	2.766	0.588	0.000	–	0.679	0.968	3.137	0.101	4.13	2.21	1.80	0.06	12.65% (1.53 σ) [2]
expc3	0.352	14.002	0.812	–	0.679	0.968	3.137	0.101	5.39	3.40	1.82	0.09	14.52% (1.46 σ) [3]
jump	0.382	–	0.829	–	0.678	0.967	3.118	0.093	5.30	4.19	1.09	–0.07	7.08% (1.81 σ) [2]

TABLE XII. Fit and γ using Planck TT , TE , EE + lowP + H0 + BAO.

$\xi(k)$	$k_c^{-1}[\text{Gpc}]$	λ	β	α	h	n_s	$\ln(10^{10}\mathcal{A}_s)$	τ	Γ	Γ_{lowP}	Γ_{highP}	Γ_{H0}	Γ_{BAO}	γ
plaw	–	–	–	–	0.681	0.970	3.123	0.095	0.00	0.00	0.00	0.00	0.00	–
bpl	0.234	0.152	–	–	0.682	0.970	3.158	0.112	4.67	2.69	1.74	0.11	0.01	9.66% (1.66 σ) [2]
atan1	6.613	1.000	0.000	1.000	0.681	0.965	3.135	0.099	3.25	3.97	–0.28	–0.16	–0.04	7.14% (1.80 σ) [1]
atan2	6.613	1.000	0.000	1.000	0.681	0.965	3.135	0.099	3.26	3.97	–0.26	–0.16	–0.04	19.54% (1.29 σ) [2]
atan3	6.613	1.000	0.000	1.000	0.681	0.965	3.135	0.099	3.28	3.97	–0.24	–0.16	–0.04	35.09% (0.93 σ) [3]
atan4	0.389	31.581	0.817	0.761	0.680	0.968	3.134	0.100	5.43	4.61	1.27	–0.40	–0.09	24.56% (1.16 σ) [4]
expc1	3.671	0.500	0.000	–	0.681	0.969	3.137	0.102	3.98	3.55	0.51	0.02	0.00	4.62% (1.99 σ) [1]
expc2	2.589	0.605	0.000	–	0.682	0.970	3.147	0.107	4.31	2.90	1.23	0.12	0.01	11.58% (1.57 σ) [2]
expc3	0.356	13.829	0.815	–	0.680	0.968	3.136	0.101	5.33	4.53	1.38	–0.50	–0.13	14.90% (1.44 σ) [3]
jump	0.381	–	0.832	–	0.681	0.969	3.124	0.095	5.14	5.13	0.23	–0.17	–0.02	7.66% (1.77 σ) [2]

Our polarization angular power spectra are also linear functionals of \mathcal{P}_s and \mathcal{P}_T and so similarly we have

$$C_\ell^{XY} = A_s C_{s,\ell}^{XY}[f] + r A_s C_{T,\ell}^{XY}[g], \quad (24)$$

where X and Y can denote the possible polarizations E and B (as well as the temperature T). If r is very small, the total values of C_ℓ^{TT} and of C_ℓ^{XY} will be determined essentially by \mathcal{P}_s only.

Now the data seem to show anomalously low values of C_ℓ^{TT} for ℓ roughly in the interval $[2, 50]$. If we modify the function $f(k)$ appropriately we can improve our fit to the TT data in this region. However, it is not so straightforward if we consider a data set that includes polarization. For example, if we take the data sets TT and $TE + EE$, the component $TE + EE$ does not have the same anomalously low power at low ℓ . Thus if we try modifying $f(k)$ so as to improve the fit to the TT data, at some point we will worsen the fit to the $TE + EE$ data. In other words, with a total likelihood

$$\ln L_{\text{total}} = \ln L_{TT}[A_s, f] + \ln L_{TE+EE}[A_s, f], \quad (25)$$

lowering the power in f will increase the first term but decrease the second, so that the best fit will be somewhere in the middle ground.

If instead the tensor contribution is not negligible on all scales of interest, it may be possible to increase $\ln L_{TT}[A_s, r, f, g]$ without decreasing $\ln L_{TE+EE}[A_s, r, f, g]$ – provided we are allowed to vary the functions f and g independently. For then we might be able to choose f such that we have lower power in C_ℓ^{TT} on large scales while at the same time choosing g such that it compensates for the lower power in C_ℓ^{TE} and C_ℓ^{EE} at large scales (resulting from lower values of $C_{s,\ell}^{TE}[f]$ and $C_{s,\ell}^{EE}[f]$) and without spoiling the rest of the fit. This would require the relative tensor contributions to TE and EE to be larger than the relative tensor contribution to TT , which can occur in appropriate conditions.

However, to vary f and g independently amounts to a violation of scalar-tensor consistency. In such conditions the definition

$$r \equiv 4 \frac{\mathcal{P}_T}{\mathcal{P}_s} \quad (26)$$

of r is no longer a fixed number but will generally depend on k . In practice, however, r is taken to be the ratio (26) at the pivot scale $k = k_*$ (with \mathcal{A}_s defined as the value of \mathcal{P}_s at $k = k_*$ so that $f = 1$ at that point), in which case the general relations (23) and (24) are still valid. Note that while this scenario requires a large contribution from tensor modes at large scales, r itself could still be small since it is defined at the relatively small pivot scale.

This reasoning suggests that, if the low-power anomaly in C_ℓ^{TT} is real, then having significant tensor contributions at large scales (with a violation of scalar-tensor consistency) might allow us to avoid a degradation of the fit when polarization data are included.

An intriguing feature of quantum relaxation models is that they naturally imply a large-scale violation of scalar-tensor consistency without spoiling the overall inflationary scenario [9]. This is because, when the initial conditions are no longer constrained by the Born rule, there is no reason why different degrees of freedom should have the same initial nonequilibrium distribution and hence there is no reason why they should have the same large-scale deficit function $\xi(k)$.⁶ In general we will have two distinct functions $\xi_s(k)$ and $\xi_T(k)$ for scalar and tensor modes respectively, with two different and unequal sets of parameters $\alpha_s, \beta_s, (k_c)_s$ and $\alpha_T, \beta_T, (k_c)_T$ (with $\lambda = 1$ throughout). A more complete data analysis would then require a fit to this six-parameter model, where for completeness r itself could also be subject to a fresh fit. Such studies are left for future work.

VI. IMPLICATIONS FOR QUANTUM RELAXATION MODELS

In this section we consider the implications of our data analysis for quantum relaxation models [6–9].

A. Best-fit results for the nonequilibrium deficit

As noted in Section II A, quantum relaxation during a radiation-dominated pre-inflationary era (combined with a simplifying assumption about the transition to inflation) predicts an approximate deficit function $\xi_{\text{neq}}(k) = 1 - \chi_{\text{neq}}(k)$, where χ_{neq} takes the form (6) with $\lambda = 1$ [6, 7]. That is, the relaxation scenario predicts the deficit function that we have here called **atan3**, with three undetermined parameters α, β and k_c . In the present analysis we have fitted the data to **atan3**, and also to the reduced functions **atan2** (with $\alpha = 1$) and **atan1** (with $\alpha = 1$ and $\beta = 0$). One may ask which of the **atan** functions provides the best fit and whether this fit provides some useful constraints or hints concerning the underlying model. The answer depends somewhat on the data sets considered, in particular on whether we consider only data sets with no polarization (Tables I–IV) or whether we instead consider only data sets that include polarization (Tables V–XII).

As a general point of principle, it could happen that a useful pattern emerges only for data sets that include polarization. More complete data sets can be required to observe an effect, where more data generally implies smaller error bars which can overcome noise. In this spirit it may be useful to consider Tables I–IV and Tables V–XII as two distinct sets of data.

⁶ See Ref. [7] for examples where different initial nonequilibrium distributions all give rise to approximately **atan** spectra but with different parameter values.

1. Best fit without polarization

If we restrict ourselves to data sets without polarization, for a reliable best fit **atan1** does not suffice and we require **atan2** or **atan3**.

To see this, observe that in Tables I–IV the parameter k_c changes considerably from **atan1** to **atan2** (where the latter fit yields quite a large $\beta \simeq 0.5$), showing that **atan1** is not a reliable fit. Thus, while **atan1** shows an apparently impressive significance of up to 2.66σ (Table II) for these data sets, the instability of the fit indicates that this result should be discounted. Whereas, again for Tables I–IV, the parameters k_c and β are more or less stable from **atan2** to **atan3** (although less stable for Table IV), suggesting that **atan2** is a reliable fit – with a significance of up to 2.41σ (Table II). The latter result is suggestive, but as we shall discuss the significance diminishes when polarization data are included.

2. Best fit including polarization

If instead we ignore data sets without polarization, we find that the only relevant parameter is the (uncertain) scale k_c , so that the best-fit function is in effect just **atan1**. However, we cannot really conclude that $\beta = 0$ because the data cannot provide such a constraint.

To see this observe that, in Tables V–XII, from **atan1** to **atan2** the parameter k_c remains stable and β acquires at most a small value (close to zero). This might seem to indicate that **atan1** (which has β fixed at 0) is a reliable fit. However, in reality β simply cannot be constrained by the data. This is because, if the deficit scale k_c^{-1} is large, the value of β can affect the spectrum in a region that in turn affects the data only if β is close to 1. (For example, if we had $\beta = 0.01$ and $k_c^{-1} = 1$ Gpc then β would affect the spectrum around $k^{-1} \sim 100$ Gpc, which is too large to affect the data.) If instead β is not close to 1, its value will not affect the fit to the data (unless the scale k_c^{-1} is much smaller, as in the jump model). In particular, if β is small the data cannot constrain its precise value. Now, in our fitting procedure for **atan2** and **atan3** (with β freely varying), the starting value of β was taken to be $\beta = 0$. The algorithm begins to explore the parameter space for β , but because small values of β do not affect the data the assigned values of β simply stay very close to zero.

If instead we began the fitting process with a larger (non-zero) value of β , it seems likely that the assigned value would diminish until it becomes so small as to be irrelevant again (though this last point remains to be checked). To go further, an MCMC analysis could provide an approximate upper bound on β . However, there would be no best-fit value as the distribution for β is roughly flat. (Figure 2 shows a correlation between β and k_c^{-1} , where any value of β between 0 and 1 is more or less equally probable.)

3. Significance of atan1

If we consider all the data sets, we find, as a rough general trend, that the more data we add the larger the best-fit lengthscale k_c^{-1} and the smaller the significance of the fit. This suggests that the effect is probably a statistical fluctuation. In principle, however, it could be that the effect only occurs at super-Hubble scales and that the **atan1** model is trying to fit a real physical feature there. With this in mind, if we allow ourselves to disregard the data sets without polarization (and if we fix $\lambda = 1$ as in the quantum relaxation model), then the following reasoning leads us to consider the one-parameter deficit **atan1**. If we begin by fitting **atan3**, we find that the data are insensitive to α and so we may as well fix its value at $\alpha = 1$ and continue with one less parameter; then we find that the data are also insensitive to β and so we may as well fix its value at $\beta = 0$ and again continue with one less parameter. Thus **atan1** may be regarded as a smooth alternative to the sharp function **jump**.

For the data sets including polarization, **atan1** is found to have a significance of up to 1.97σ (Table VIII), which is insufficient to count against the null hypothesis. This is comparable to, if slightly better than, the significance of **jump** for the same data sets (up to 1.92σ , Table IX). For data sets without polarization, as we have noted **atan1** yields a significance of up to 2.66σ (Table II), while by comparison **jump** yields a significance of only up to 2.20σ (for the same data set). Despite this difference, however, **jump** has the quite remarkable property of yielding stable parameters across all data sets, thereby motivating the follow-up Bayesian analysis carried out below. The case for running a similar Bayesian analysis for **atan1** is not as strong and hence we leave this for future work.

B. Quantum relaxation and future work

We now comment on the implications of our results for future work on quantum relaxation models.

1. Mechanism for negligible super-Hubble power

As far as p -values are concerned, **atan1** performs more or less as well as **jump** (for data sets including polarization). This motivates us to ask if there might be a theoretical model that predicts **atan1** and in particular a near-vanishing β . Because $\beta = \lim_{k \rightarrow 0} \xi_{\text{neq}}(k)$, this means that we require a model in which the primordial power spectrum itself becomes negligible in the far super-Hubble limit.

In a quantum relaxation scenario with a radiation-dominated pre-inflationary phase, the limit $k \rightarrow 0$ yields the maximum suppression or ‘freezing’ of quantum relaxation. As shown in Section V of Ref. [8], in the far

super-Hubble regime the de Broglie-Bohm time evolution of a field mode on an interval (t_i, t_f) with $t_f \gg t_i$ is equivalent to the time evolution of a standard harmonic oscillator on a time interval $(t_i, 3t_i)$. Thus for $k \rightarrow 0$ all modes effectively evolve over the same small time $2t_i$ and we expect very limited relaxation. At small k the resulting deficit function $\xi_{\text{neq}}(k)$ will then be essentially equal to the deficit function $\xi_{\text{ic}}(k)$ associated with the initial conditions. This means that, for long-wavelength modes, the freezing of relaxation preserves the initial conditions almost intact. A negligible value of β then implies a negligible statistical variance (or power) in the initial conditions themselves (for modes in the far super-Hubble regime).

This motivates us to consider a quantum relaxation scenario in which there is negligible super-Hubble noise in the initial state (corresponding to very small β). It is a matter for future theoretical work to develop the details of such a scenario. A simple suggestion is to assume that there is negligible power in the initial conditions for all modes. This is an attractive hypothesis, as physically it means that essentially all of the quantum noise we observe at later times was generated dynamically⁷.

While the hypothesis of negligible initial power provides a good physical reason to prefer **atan1**, so far the significance remains small. A full MCMC analysis might help to evaluate whether or not it is worth pursuing such models. This would depend on the resulting upper bound on β .

If this hypothesis is considered further, it would be natural to apply the same reasoning to tensor modes as well, in which case we would expect the distinct functions $\xi_{\text{S}}(k)$ and $\xi_{\text{T}}(k)$ (discussed in Section V C) to each take the form of **atan1** but with different scales $(k_{\text{c}})_{\text{S}}$ and $(k_{\text{c}})_{\text{T}}$ (again generally breaking scalar-tensor consistency).

2. Other signatures of quantum relaxation

The data seem to show that if there is a low-power anomaly it must exist at large scales that we cannot accurately measure. The data are too noisy in the relevant region to meaningfully test the predictions of quantum relaxation for the power deficit alone. To improve the chances of constraining such models we need to include more detailed predictions – such as primordial oscillations and statistical anisotropy, which are additional generic features of quantum relaxation. Extensive numerical simulations show significant oscillations around the **atan** function [6, 7], which have however so far

eluded a simple and general parameterization. Statistical anisotropy arises from initial nonequilibrium distributions that depend on the direction $\hat{\mathbf{k}}$ of the wave vector, resulting in parameters $\alpha, \beta, k_{\text{c}}$ that depend on $\hat{\mathbf{k}}$, where the effect of $\alpha(\hat{\mathbf{k}})$ could arguably persist at large ℓ and hence have a more visible impact on the data [35].

3. Quantum relaxation across the transition

Finally, it should be emphasised that the **atan** prediction was obtained on the simplifying assumption that the transition does not affect the nonequilibrium distribution left at the end of a radiation-dominated pre-inflationary era [6]. Modeling the transition and simulating the time evolution of nonequilibrium across it remains to be done. How this might change the overall result is currently unknown. The evidence we discuss below in favour of a sudden **jump** deficit raises the question of whether or not a realistic quantum relaxation model could yield such a result (or, indeed, if such a result could arise from other kinds of models not involving quantum relaxation).

VII. THE JUMP FUNCTION

Having found that a smooth transition to large-scale low power does not improve the fit to a degree that is convincingly significant, we now consider the extreme case of a sharp transition. More precisely, we discuss a transition that is so fast that the data are incapable of discerning its structure. Statistically speaking one could argue, from the results in our Tables, that the jump case is not necessarily preferable to some of our other models such as **atan1** or **expl**. However, one should bear in mind that the latter cases correspond to imposing strong priors on the extra parameters and with no particular physical justification (though see Section VI for a possible physical motivation for **atan1**). Moreover, as a careful investigation of the Tables reveals, the jump model appears to be remarkably stable with respect to the data set considered, in contrast with the other models. In particular, the values of the jump parameters vary little from one data set to another (the statistical significance of the fit being also somewhat more stable). Finally it should be emphasized that, starting from a smooth transition, the likelihood minimization procedure itself naturally leads us to a sharp transition. It is in this sense that we view the **jump** deficit proposal as being suggested in an especially natural way by the data.

For practical purposes we regard the transition as instantaneous, amounting to a jump or discontinuity in the primordial power spectrum. In Fig. 5 we show the difference between the sharp **jump** deficit and the smooth **plaw** and **atan1** deficits, together with the consequences for the matter power spectrum $P_{\text{m}}(k)$. Figure 6 shows that, when translated into CMB anisotropies, the **jump** deficit decreases the C_{ℓ} 's at larger multipoles than is the

⁷ In Ref. [9, Sec. X] it was argued that, in a theory of dynamical quantum relaxation, it is natural to have an initial subquantum width (so that $\xi_{\text{ic}}(k) < 1$). Following the same logic to its conclusion, it is arguably natural to take $\xi_{\text{ic}}(k)$ to be as small as possible and to set $\xi_{\text{ic}}(k) \simeq 0$.

case for the smooth deficits **plaw** and **atan1**. Specifically, **jump** produces a larger angular-power deficit in the region $\ell = 20\text{--}30$.

As we have noted, the case of a sharp transition exhibits an intriguing stability across our data sets. For C_ℓ^{TT} only, we obtain a variation of less than 2% for the best-fit characteristic scale k_c^{-1} , which is found to range from 353 to 361 Mpc, and we find a best-fit dip in power down to between 76 and 79% (that is, we find β between 0.76 and 0.79). The p -value is around 3%.

Including the polarization for the low multipoles increases the p -value to around 10%, while increasing the scale k_c^{-1} to about 370 Mpc and leaving the dip β essentially unchanged at around 0.80 or 80%. With the full polarization data the scale is pushed upward even more, reaching about 380 Mpc, while the dip reaches 83% at most and the p -value is lowered to 7%. Thus it would appear from the data that we are unable to unambiguously assert the existence of a new characteristic length scale, although our analysis naturally points to one. Even so, as shown in Fig. 3, this variation in the value of the scale is well within the error bar for k_c^{-1} .

As we can see in Fig. 2 the distribution for k_c^{-1} has at least two modes, the first at 378 Mpc and the second at 3291 Mpc. The former represents the sharp transition and the latter represents the smooth one. Note that the second mode turns into a plateau where the distribution is completely degenerate (as expected at such scales). In the second corner plot (Fig. 3) we focus on the first mode, removing all points $k_c^{-1} > 800$ Mpc from the posterior sample. Focusing on the first mode also affects the values of A_{SA} and z_{re} , preferring a larger amplitude and earlier reionization.

Finally, we have computed the Bayes factor for the comparison of **jump** and **plaw**. As stated before, we use flat priors for the cosmological parameters together with the PFI priors. For nested models, the priors of the common parameters do not change the final Bayes factor (see for instance Ref. [37]). The only relevant priors are those for the new parameters:

$$-1 \leq \ln \left(\frac{k_c^{-1}}{1 \text{ Mpc}} \right) \leq 18, \quad 0 \leq \beta \leq 1.$$

Instead of reporting a single value for B_{FA} for the above priors, we adopt the framework of a robust Bayesian analysis. The prior of β is chosen so that all possible deficits are allowed and are equally probable. However, there is no clear way to choose a meaningful interval for the prior of $\ln(k_c)$. We circumvent this problem by calculating the Bayes factor for all subintervals of $-1 \leq \ln \left(\frac{k_c^{-1}}{1 \text{ Mpc}} \right) \leq 18$ and plotting the results in Fig. 4, thereby showing the sensitivity to the prior. The Bayes factor for the full interval is found to be

$$B_{\text{FA}} = 10^{1.33} = 21.6.$$

This is considered ‘strong’ on the scale given in Ref. [36, Appendix B].

In Fig. 4 there is no interval where the evidence is ‘decisive’ or ‘very strong’, although in a large portion of the graph the Bayes factor is classified as ‘strong’. On the other hand, for the evidence to be ‘strong’ it is necessary that both peaks in the distribution of k_c^{-1} be allowed by the prior (see Fig. 2). For priors including the first or second peak only, the evidence drops to ‘substantial’. The figure shows that to achieve ‘strong’ evidence it is necessary to include both peaks or the second peak and part of the plateau. Thus a conservative conclusion is that we have only ‘substantial’ evidence for a particular scale (at $k_c^{-1} = 3291$ Mpc or at $k_c^{-1} = 378$ Mpc).

VIII. CONCLUSIONS

A smooth deficit function can be superimposed on the primordial power spectrum to mimic the large-scale deficit which has apparently been observed in some cosmological data. We have analyzed a broad range of data using different parameterized versions of the deficit function, in such a way as to be able to compare with a previous analysis by the Planck team. We confirm that, for the deficit functions we consider, the fit is only marginally better than for the standard power law, where the improvement occurs at wavelengths comparable to the Hubble scale. It would appear that, taken by itself, the power deficit is not very statistically significant and therefore not necessarily physical. This result is consistent with previous investigations. We do, however, find some suggestive hints for future work.

We have consistently found hints of statistically-significant fits, only to find that the significance degrades when polarization data are added. We have argued that such degradation might be avoided in models that break scalar-tensor consistency and which have non-negligible tensor contributions at large scales. Quantum relaxation models in fact naturally break scalar-tensor consistency, yielding independent deficit functions for scalar and tensor degrees of freedom. Fitting such extended models to the data may be considered in future work. Another possibility, however, is that our fits without polarization are partially over-fitting noise in those data sets, so that when polarization data are added this part of the modeling loses its significance.

The behavior of the restricted (one-parameter) quantum relaxation deficit function **atan1** across all data sets arguably suggests that it is merely modeling a statistical fluctuation, since adding more data tends to increase the lengthscale k_c^{-1} and decrease the significance. Possibly, however, the fit is trying to capture a real feature at super-Hubble scales. To test this, we might consider disregarding the data sets without polarization, in which case our results do suggest that **atan1** may be worth considering further, in particular because the data seem to be relatively insensitive to the values of the additional parameters α and β . Physically, the function **atan1** has vanishing power in the far super-Hubble limit, and we

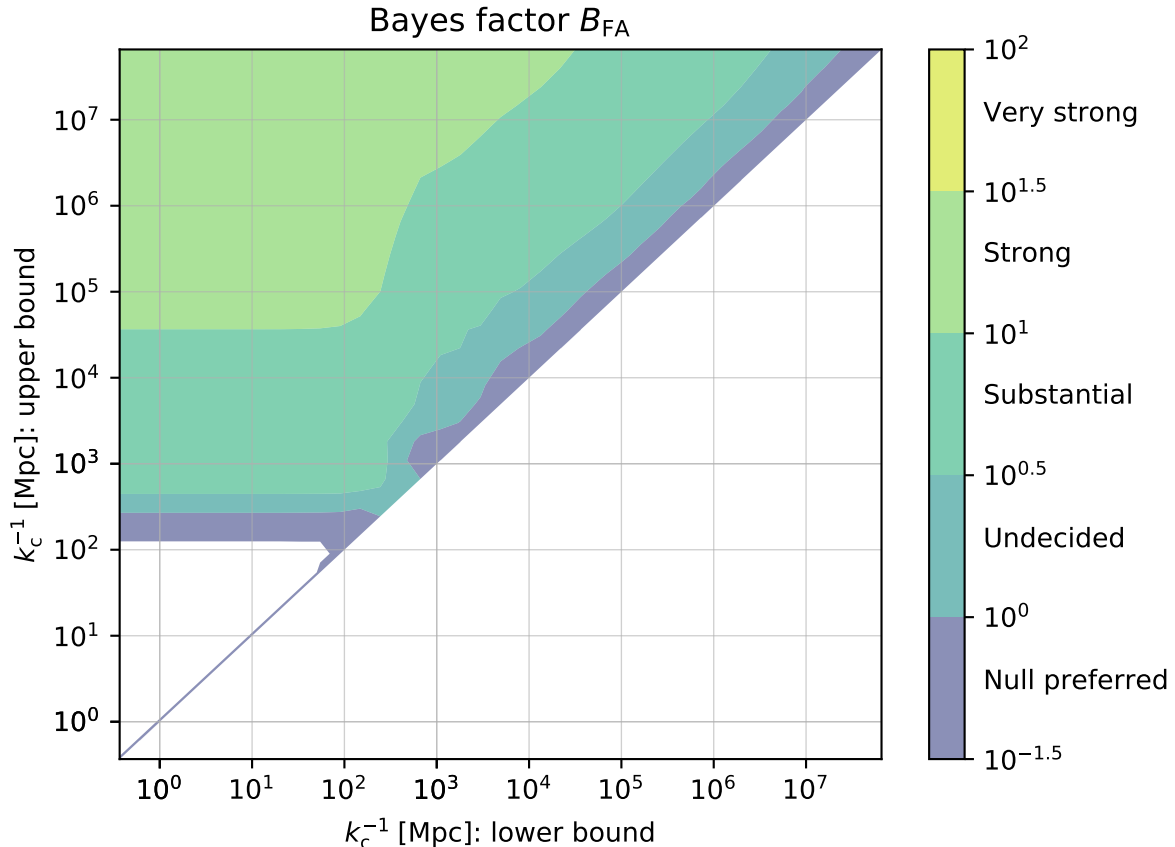


FIG. 4. Bayesian evidence for various combinations of upper and lower bounds on k_c^{-1} . The white areas represent forbidden regions (lower bound greater than upper bound) or regions without enough points in the sample. To the right of the graph we include the evidence scale proposed in Ref. [36, Appendix B].

have argued that this would be a natural feature in quantum relaxation models with negligible power in the initial conditions.

Future theoretical work on the power deficit should, however, also take note of the following elementary point. Because of the low statistical significance of the deficit, an effective test of theoretical models will require that we include further predictions such as primordial oscillations or statistical anisotropy, especially if these are able to affect the data at larger values of ℓ .

Our study of smooth deficit functions has, however, already led us to an unexpected and statistically significant result of another kind. By allowing the fit to run on the characteristic deficit speed, we have found that the additional power index – the parameter λ in (8) – is naturally driven to very large values, implying an almost discontinuous or step-like deficit function. After having scanned much of the parameter space, we studied the specific case which the data seemed to be pointing to: a deficit function **jump** with only two parameters, specifically a break point k_c indicating the scale above

which the usual fiducial power spectrum is valid and a relative amplitude difference β . Running our analysis with this two-parameter step function (21), we obtained a fit with better (in the sense of more stable parameters) agreement with the full range of data sets, exhibiting a new length scale D_c around 350 Mpc today and with a power deficit of about 20%. This stability indicates that the model is not merely over-fitting noise in a particular data set, and that the feature it fits is real. The resulting modification of the primordial power spectrum and its impact on the matter power spectrum are shown in Fig. 5. In our Bayesian follow-up analysis we obtained ‘strong’ evidence when allowing the scale to vary in a wide interval and ‘substantial’ evidence for our peak at around 350 Mpc.

Taking D_c at face value today, and running it backwards by some appropriate number N of e-folds to an inflationary phase during which it may have been generated, we find a corresponding primordial scale around $\ell_c \sim 5 \times 10^7 e^{120-N} \ell_p$, with ℓ_p the Planck length. For the commonly quoted value $N = 120$ (including the later

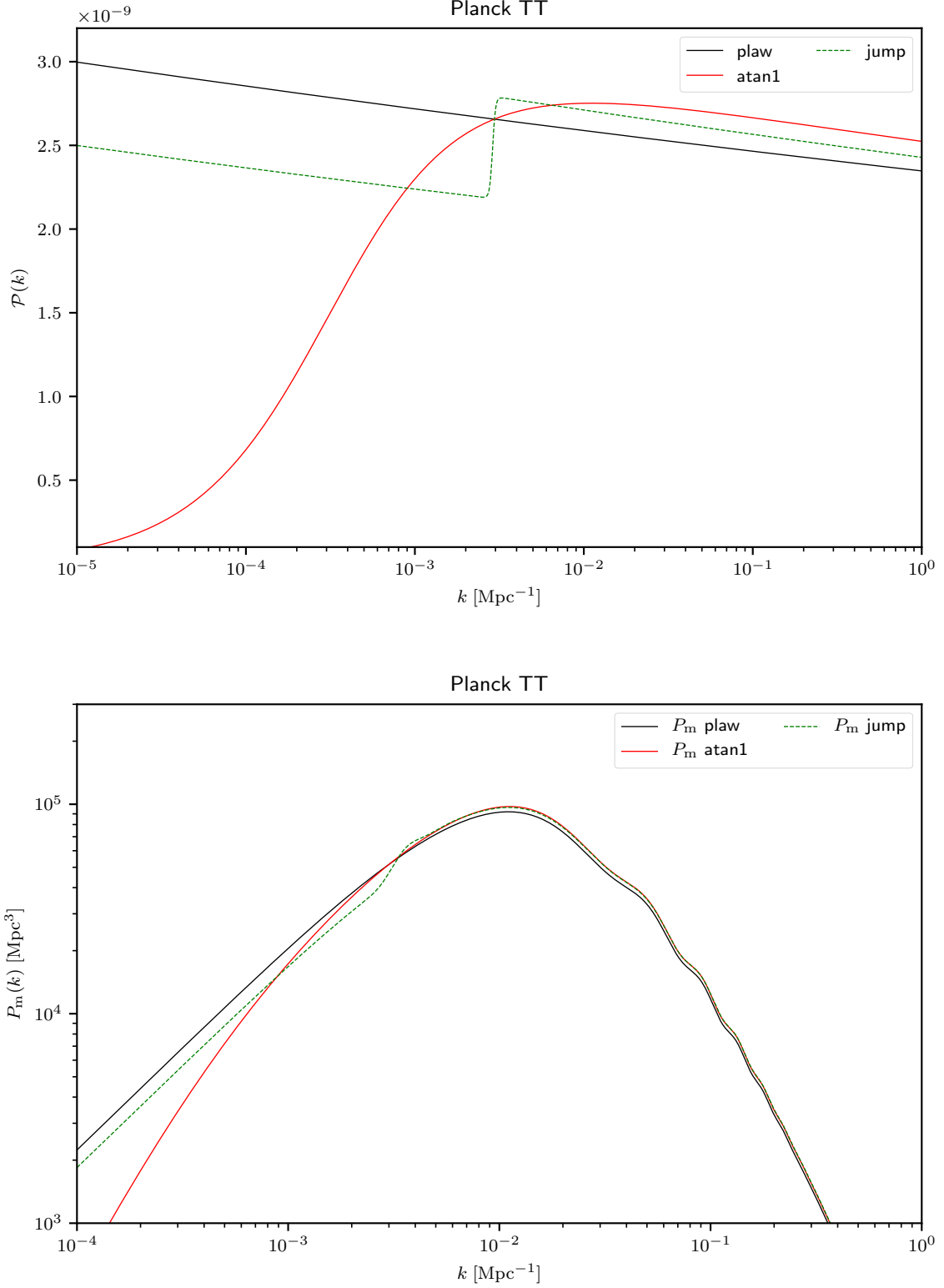


FIG. 5. Upper panel: best-fit power spectra with the most successful deficit functions (see text). It is clear that for a smooth transition the relevant scale at which the deficit becomes significant is of order the Hubble radius, whereas in the almost discontinuous case (with a large value of λ) the transition scale is an order of magnitude smaller. Lower panel: the corresponding matter power spectra. Only the case of a sharp transition remains close to the case of a fiducial spectrum. It is an open question to understand if and how such a slight difference could be observable in future data. These fits are for the data sets including Planck TT only.

radiation- and matter-dominated epochs), in terms of energy this scale corresponds to $\approx 2.4 \times 10^{20}$ eV. If N is allowed to range up to ~ 136 , the scale approaches ℓ_p or an energy scale $\sim 10^{19}$ GeV. Forthcoming experiments may yield further insights into the magnitude, statistical significance, and physical relevance of this potentially new scale.

ACKNOWLEDGMENTS

PP and SDPV would like to thank the Labex Institut Lagrange de Paris (reference ANR-10-LABX-63), part of the IDEX SUPER, within which this work was partly done. SDPV would like to acknowledge financial aid from the CNPq PCI/MCTI/CBPF program, PNPd/CAPES (Programa Nacional de Pós-Doutorado/Capes, reference 88887.311171/2018-00) and financial support from a BELSPO non-EU postdoctoral fellowship. PP is hosted at Churchill College, Cambridge, where he is partially supported by a fellowship funded by the Higher Education, Research and Innovation Dpt of the French Embassy to the United-Kingdom. AV is grateful to Murray Daw and Mark Leising at Clemson University for their support during this project.

This research also made use of the MeSU supercomputer of the Université Pierre & Marie Curie. The university policy changed while this work was being done, so the MeSU supercomputer became too complicated to use. We therefore switched to the Horizon Cluster funded by the Institut d’Astrophysique de Paris. We thank Stéphane Rouberol for running this cluster smoothly for us.

We would also like to thank R. Trotta for a careful reading of the manuscript and for many suggestions for improvements.

Appendix A: NumCosmo

In this appendix we briefly describe the numerical tools used in this work. These tools are part of the Numerical Cosmology library – NumCosmo [38]. All codes described here are located in the project’s repository <https://github.com/NumCosmo/NumCosmo> and the library’s documentation is in <https://numcosmo.github.io/>. The library contains an independent implementation of several tools used in numerical cosmology, providing a complete toolkit to compute and analyze different cosmological observables. The observables were computed with the homogeneous and isotropic cosmological models objects (NchiCosmo*) and with the Boltzmann code using CLASS [31–33] as back-end. Different precision files were used, all based on `chi2pl0.01.pre` (which was calibrated by the CLASS developers to provide a 10^{-3} error in C_ℓ). This precision file was modified to increase the number of points per decade to evaluate the PPS and to decrease the distance

between interpolation points in ℓ (no interpolation for low- ℓ and increasing interpolation for high- ℓ). This was necessary to capture the features added by the different deficit functions. We used three different precisions, the default CLASS precision (LP), the `chi2pl0.01.pre` file with the points per decade on the PPS increased to 50 (MP), and HP with the same file as MP but including also the modification of the interpolation for ℓ . After running the best-fit finder using these precisions, we found no relevant differences between MP and HP.

For the best-fit finders we used NumCosmo’s `NcmFit` object and the `NLOpt` (see Ref. [39]) library as the minimization library back-end. We tested different numerical optimization algorithms. The most efficient and stable algorithms found were the Nelder-Mead [40–42] and Subplex [43]. The main advantage of these algorithms is that they do not require the objective function derivatives and have a better handling for discontinuous functions. The likelihood used is, in principle, a smooth function of the parameters θ , although the computation of C_ℓ^{XY} introduces numerical errors in the evaluation of $L(D|\theta)$, which in turn can create artificial discontinuities at the error level. Accordingly, any optimization algorithm that depends on the smoothness of the likelihood (for example, some algorithms create a cubic approximation to the objective function or calculate an estimate of the derivative through finite differences) will find spurious maxima resulting from these small discontinuities. In our fitting process we found that even the more appropriate algorithms terminate prematurely due to the artificial maxima. For this reason, we rerun the fitting process iteratively until the last two minima coincide within a 0.1% margin. This process was automated in the `NcmFit.run_restart` method.

We note a small difference between the parameter best-fit values using different precisions for the CMB anisotropies and/or accuracy for the minimization algorithm. The code used by Planck, `CosmoMC` [44, 45], uses the BOBYQA [46] as the best-fit finder or even the point with smaller $-2 \ln(L)$ value found during the MCMC exploration. We also tested these two methods. Both provide sub-optimal minima with small differences in the best-fit parameters.

The MCMC algorithm used is identical to that used in appendix D of Ref. [47]. Note however that, in our analysis, we did not use the profile likelihood for the PFI parameters: instead, we used a complete sample including all parameters. In appendix E of Ref. [47], one can find the description of all the diagnostics used to assert the convergence of the MCMC sampler.

Finally, we used the harmonic mean (see for context [48]) to estimate the evidence integral. In our implementation, our posterior sample was obtained from the MCMC to compute the integral

$$\langle g(\theta) \rangle = \int d\theta g(\theta) P(\theta|\mathcal{M}, D) \approx \frac{1}{N} \sum_i g(\theta_i),$$

where θ_i are the N points in the posterior MCMC sample.

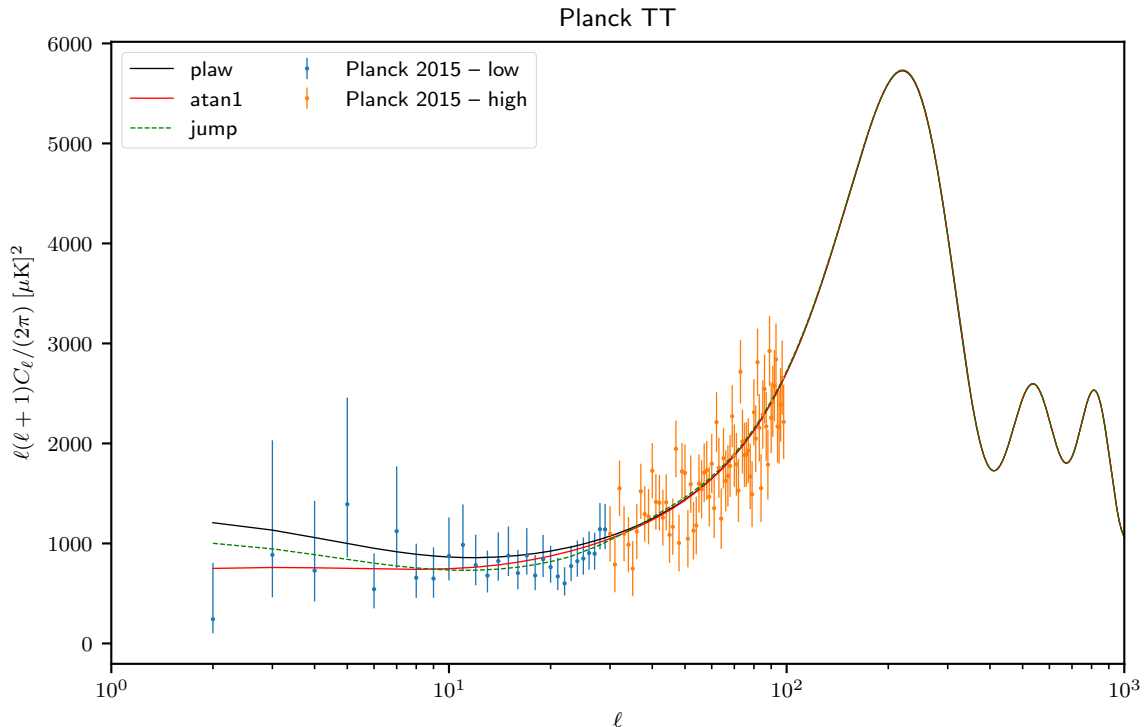


FIG. 6. Examples of best-fit CMB anisotropies with the different deficit functions (see text), together with the Planck 2015 TT data up to $\ell = 100$ (this limit chosen for aesthetic reasons). The smooth transition represented by **atan1** results in a larger deficit at the lower multipoles ($\ell = 2-10$), whereas **jump** results in a deficit which is smaller at these lower multipoles and larger at the higher multipoles $\ell = 20-30$. This reveals the difference between the sharp and the smooth deficit. The latter improves the fit at the lowest multipoles only, while the former also affects the spectrum around $\ell = 20-30$ where the cosmic variance is less important.

Using Bayes theorem we have

$$\int d\theta g(\theta) \frac{P(\theta|\mathcal{M})L(D|\theta, \mathcal{M})}{P(D|\mathcal{M})} \approx \frac{1}{N} \sum_i g(\theta_i),$$

where $L(D|\theta, \mathcal{M})$ is the likelihood and $P(\theta|\mathcal{M})$ the priors. We usually do not know the properly normalized likelihood $L(D|\theta, \mathcal{M})$, thus we define $L'(D|\theta, \mathcal{M}) \equiv N_L L(D|\theta, \mathcal{M})$, as the unnormalized likelihood (which is used in most cases for MCMC), and N_L the normalization factor (which does not depend on any parameter), where the value of $P(\theta|\mathcal{M})L'(D|\theta, \mathcal{M})$ was the one used by the MCMC sampler. For this reason we can choose

$$g(\theta) = \frac{F(\theta)}{P(\theta|\mathcal{M})L'(D|\theta, \mathcal{M})},$$

to obtain

$$\frac{1}{N_L P(D|\mathcal{M})} \int d\theta F(\theta) \approx \frac{1}{N} \sum_i \frac{F(\theta_i)}{P(\theta_i|\mathcal{M})L'(D|\theta_i, \mathcal{M})}.$$

We then choose $F(\theta)$ to be a multivariate normal distribution with the mean and covariance equal to the estimates from the MCMC sample θ_i . However, the support

of $F(\theta)$ must be the same as that of $P(\theta|\mathcal{M}, D)$ and therefore we normalize $F(\theta)$ in the same domain as $P(\theta|\mathcal{M}, D)$ obtaining a truncated multivariate normal distribution. After the normalization we finally get our estimator for the reciprocal of $P(D|\mathcal{M})$ (modulo the irrelevant constant factor N_L):

$$\hat{Z} \equiv \frac{1}{N_L P(D|\mathcal{M})} \approx \frac{1}{N} \sum_i \frac{F(\theta_i)}{P(\theta_i|\mathcal{M})L'(D|\theta_i, \mathcal{M})}.$$

We computed the error in \hat{Z} using two methods. The first consists in splitting the sample θ_i into M subsamples, computing \hat{Z}_i for each one, and from the results computing estimators for the mean and variance. The second method consists in bootstrapping θ_i (re-sampling with replacement), computing \hat{Z}_i for each bootstrap realization, and applying the usual mean and variance estimators. Both methods give numerically equivalent results.

Appendix B: Model tables

In this appendix, we discuss the information already present in Tables I to XII but ordered differently so as to allow an easy model-by-model comparison with respect to various data sets. Additionally, we briefly discuss the performance of each model with respect to all data sets used.

1. Broken power-law: **bpl**

The **bpl** model defined by the deficit function (5) has only two degrees of freedom, namely the scale at which the power law changes and the amount by which it changes at that scale. It is not capable of producing a strong variation in the amplitude of the PPS, unless there is a drastic variation of the spectral index. The **bpl** values fitted for the different data sets we considered are shown in Tab. XIII, and we can directly observe three different behaviors: first, fitting temperature only (lines 1 through 4) favors a strong cut at an almost Hubble scale, and then with a very large spectral index change, of order ≈ 8 . Second, low- ℓ polarization reduces the characteristic scale to being sub-Hubble and yields a more reasonable ≈ 0.7 change in the spectral index. Finally, when polarization at both low- ℓ and high- ℓ are included, the new scale is reduced even more (to about 220 Mpc) but the change in the spectral index is reduced to ≈ 0.14 .

This simple model analysis yields some interesting conclusions. First, inclusion of H0 and/or BAO data do not alter the results in any statistically significant way, and the value of Γ varies very little when these other data are added to those from the CMB. Second, the power deficit on large scales comes, as is well-known, from temperature data alone. Therefore, when polarization is included, it is natural to expect the temperature deficit to disagree with polarization data, and indeed we observe that the best fit not only moves to smaller scales but also acquires a much reduced change in the spectral index. The low- ℓ data set alone moves the characteristic scale by a small amount, but the increase of the spectral index is heavily reduced. When all polarization data are included, the deficit moves to an even smaller scale with an almost negligible variation of the spectral index.

Note that the C_ℓ^{XY} are integrals of the PPS over k , so that a deficit at small k (large scales) can modify the values of C_ℓ^{XY} in a finite range. When temperature alone is considered, this can be compensated for by a relative increase of the spectrum amplitude, as is indeed seen in the first four lines of Table XIII where the amplitude is slightly increased by a factor of 6-10% in these cases.

Finally, we remark that none of the **bpl** fits yields a significant improvement when compared to the fiducial model. This means that such a simple modification in the power law does not provide a better fit.

2. Inverse tangent models: **atan1-4**

The **atan** model given by Eq. (8) provides a very smooth deficit correction to the fiducial PPS. In fact, the parameter k_c is not really a characteristic scale in this case, as can be seen by the following example: setting $\beta = 0$, $\alpha = 1$ and $\lambda = 1$, one obtains the following values for $X_\xi \equiv k/k_c$

$$X_{1\%} = 0.01, \quad (\text{B1})$$

$$X_{5\%} = 0.07, \quad (\text{B2})$$

$$X_{20\%} = 0.33, \quad (\text{B3})$$

$$X_{80\%} = 4.3, \quad (\text{B4})$$

$$X_{95\%} = 19, \quad (\text{B5})$$

$$X_{99\%} = 99, \quad (\text{B6})$$

where the index indicates the amplitude reduction compared to the fiducial PPS.

In words, Eqs. (B1) to (B6) show that ξ_{neq} starts decreasing the amplitude of the PPS already for, say, $X_{99\%} = 99$, which implies $k_{99\%}^{-1} = k_c^{-1}/99$. Therefore, for a fit with $k_c^{-1} \approx 3.5$ Gpc say, the modification starts around ≈ 35 Mpc, the power drop reaching 20% for $k_{80\%}^{-1} = k_c^{-1}/4.3 \approx 914$ Mpc. Moreover, the total deficit window can be very wide: in the case at hand, one has $X_{99\%}/X_{1\%} \approx 10^4$, so that k varies over four orders of magnitude within the deficit window. A more conservative window, from 20% to 80% say, leads to $X_{80\%}/X_{20\%} \approx 13$, which still requires a full order of magnitude variation of k . When $\beta \neq 0$, the only difference is that the deficit window ends, roughly, when $X < X_\beta$.

Table XIV summarizes our findings for **atan1**. In this case, we observe that adding polarization data has an effect opposite to what we found for **bpl**, with the value of k_c^{-1} getting larger as we include more polarization data sets (independently of the other data sets used, H0 and/or BAO). This occurs because the deficit actually worsens the polarization fit, so the effect needs be reduced in order to improve the temperature fit without spoiling the polarization fit. Since this model has a single parameter, the only way to achieve that is by pushing this parameter to a larger scale. Similarly to **bpl**, when using temperature data only, the larger deficit is compensated for by a 15-20% increase in the spectrum amplitude.

The effects of letting β vary freely (**atan2**) are shown in Table XV. For temperature data only, the fit leads to $\beta \approx 0.5$ and moves the deficit to smaller scales, from ≈ 3.5 Gpc to ≈ 1.5 Gpc, reasonably improving the fits in the process. This indicates that the deficit function acts on a smaller range and preferentially on smaller scales. When polarization data are added, the behavior already observed with **atan1** repeats itself, the deficit being pushed to larger scales. At these scales, $\beta \neq 0$ requires β of order unity to have observable consequences, but this affects the PPS at all scales in a way that disagrees with the overall CMB measurements. That is why,

TABLE XIII. Model: **bpl**.

data-set	k_c^{-1} [Gpc]	λ	β	α	h	n_s	$\ln(10^{10}\mathcal{A}_s)$	τ	Γ	γ
Planck TT	2.867	7.873	–	–	0.687	0.976	3.199	0.135	2.71	25.76% (1.13 σ) [2]
Planck TT +H0	2.812	7.582	–	–	0.703	0.986	3.245	0.162	2.62	26.93% (1.10 σ) [2]
Planck TT +BAO	2.803	7.961	–	–	0.684	0.975	3.196	0.133	2.64	26.76% (1.11 σ) [2]
Planck TT +H0+BAO	2.960	7.919	–	–	0.689	0.977	3.201	0.136	2.60	27.23% (1.10 σ) [2]
Planck TT +lowP	1.158	0.678	–	–	0.679	0.969	3.132	0.100	2.15	34.16% (0.95 σ) [2]
Planck TT +lowP+H0	1.173	0.714	–	–	0.692	0.977	3.142	0.107	2.93	23.11% (1.20 σ) [2]
Planck TT +lowP+BAO	1.187	0.627	–	–	0.681	0.970	3.124	0.096	2.32	31.40% (1.01 σ) [2]
Planck TT +lowP+H0+BAO	1.164	0.694	–	–	0.686	0.973	3.134	0.102	2.85	24.04% (1.17 σ) [2]
Planck TT , TE , EE +lowP	0.215	0.137	–	–	0.674	0.965	3.139	0.101	4.69	9.56% (1.67 σ) [2]
Planck TT , TE , EE +lowP+H0	0.223	0.142	–	–	0.680	0.969	3.144	0.105	4.78	9.17% (1.69 σ) [2]
Planck TT , TE , EE +lowP+BAO	0.234	0.144	–	–	0.678	0.968	3.143	0.104	4.74	9.36% (1.68 σ) [2]
Planck TT , TE , EE +lowP+H0+BAO	0.234	0.152	–	–	0.682	0.970	3.158	0.112	4.67	9.66% (1.66 σ) [2]

TABLE XIV. Model: **atan1**.

data-set	k_c^{-1} [Gpc]	λ	β	α	h	n_s	$\ln(10^{10}\mathcal{A}_s)$	τ	Γ	γ
Planck TT	3.587	1.000	0.000	1.000	0.696	0.975	3.303	0.185	5.50	1.90% (2.35 σ) [1]
Planck TT +H0	3.016	1.000	0.000	1.000	0.709	0.982	3.350	0.212	7.06	0.79% (2.66 σ) [1]
Planck TT +BAO	3.458	1.000	0.000	1.000	0.687	0.970	3.301	0.182	4.57	3.25% (2.14 σ) [1]
Planck TT +H0+BAO	3.896	1.000	0.000	1.000	0.691	0.972	3.279	0.172	5.57	1.82% (2.36 σ) [1]
Planck TT +lowP	5.269	1.000	0.000	1.000	0.678	0.963	3.151	0.106	3.47	6.25% (1.86 σ) [1]
Planck TT +lowP+H0	5.609	1.000	0.000	1.000	0.691	0.970	3.160	0.114	3.80	5.12% (1.95 σ) [1]
Planck TT +lowP+BAO	5.274	1.000	0.000	1.000	0.681	0.965	3.160	0.112	3.54	6.01% (1.88 σ) [1]
Planck TT +lowP+H0+BAO	5.719	1.000	0.000	1.000	0.685	0.967	3.146	0.105	3.87	4.92% (1.97 σ) [1]
Planck TT , TE , EE +lowP	6.491	1.000	0.000	1.000	0.673	0.960	3.129	0.094	3.36	6.69% (1.83 σ) [1]
Planck TT , TE , EE +lowP+H0	7.297	1.000	0.000	1.000	0.680	0.965	3.130	0.096	3.19	7.39% (1.79 σ) [1]
Planck TT , TE , EE +lowP+BAO	7.007	1.000	0.000	1.000	0.678	0.964	3.128	0.095	3.19	7.39% (1.79 σ) [1]
Planck TT , TE , EE +lowP+H0+BAO	6.613	1.000	0.000	1.000	0.681	0.965	3.135	0.099	3.25	7.14% (1.80 σ) [1]

starting from $\beta = 0$, we find that it fluctuates around zero when we add polarization.

Letting α run freely does not add much to the **atan** models. As can be seen in Table XVI this hardly improves the fits at all, as one would expect since α merely changes (and then only slightly) the shape of the deficit function. Indeed, the data remain silent about the value of α . The conclusions regarding **atan2** hold mostly unchanged for **atan3**.

The minimization procedure led to large values of λ , for which the numbers shown in the numerical example Eqs. (B1)–(B6) are no longer valid (the relationship between k_c and the range where the deficit is important being modified). The correct values are found simply by setting $X' \equiv X^\lambda$, with X' taking the same values as X in Eqs. (B1)–(B6), that is, $X_p = (X'_p)^{1/\lambda}$ for a given fraction p . For a very large value for λ , the range where the deficit is measurable collapses around k_c : for $\lambda = 40$, one has $X_{1\%} = (0.01)^{1/40} = 0.9$ and $X_{99\%} = (99)^{1/40} = 1.12$, so that the deficit function reduces the spectrum from 99% to 1% in the range $[k_c/1.12, k_c/0.9]$. This is more like a sharp jump at k_c^{-1} than a smooth transition.

Having said this, let us examine the **atan4** results displayed in Table XVII. We first note that almost all the fits prefer a very large value for λ , with the notable ex-

ception of the data set Planck TT + H0. This means that almost all fits are improved by considering a very short deficit range. This was not expected but turns out to yield remarkably stable values for k_c and β . For such short ranges any attempt to measure the deficit shape is unrealistic and the parameter α is completely degenerate, or irrelevant, in these cases. One can go even further in the analysis, as the parameter λ is also irrelevant: it merely tells us that the data prefer a sharp jump, regardless of the actual numerical value obtained for λ^8 . As already mentioned, the only exception to this was obtained when fitting Planck TT + H0. In this case, one obtains a broad deficit function acting on large scales and improving both the temperature and H0 fits simultaneously. We shall not consider this anomaly as it is found only for one specific combination of the existing data sets.

In retrospect, we realize that the sharp transition could be seen in the **atan2** fits as well, since these show a preference for smaller scales and smaller deficits. For example, for fits with temperature only, we had $k_c^{-1} \approx 1.5$ Gpc and consequently $k_{c,80\%}^{-1} \approx 350$ Mpc, a result

⁸ We have tested this by fitting the data with increasing values of λ . We obtained virtually the same results in all cases.

TABLE XV. Model: **atan2**.

data-set	k_c^{-1} [Gpc]	λ	β	α	h	n_s	$\ln(10^{10}\mathcal{A}_s)$	τ	Γ	γ
Planck TT	1.436	1.000	0.489	1.000	0.703	0.971	3.370	0.216	5.82	5.45% (1.92 σ) [2]
Planck $TT+H0$	1.326	1.000	0.504	1.000	0.712	0.975	3.391	0.227	8.27	1.60% (2.41 σ) [2]
Planck $TT+BAO$	1.981	1.000	0.477	1.000	0.688	0.964	3.305	0.181	5.02	8.12% (1.74 σ) [2]
Planck $TT+H0+BAO$	2.579	1.000	0.486	1.000	0.692	0.969	3.279	0.171	5.75	5.64% (1.91 σ) [2]
Planck $TT+lowP$	5.194	1.000	0.010	1.000	0.676	0.962	3.150	0.105	3.52	17.20% (1.37 σ) [2]
Planck $TT+lowP+H0$	5.438	1.000	0.007	1.000	0.691	0.970	3.160	0.114	3.85	14.57% (1.46 σ) [2]
Planck $TT+lowP+BAO$	5.274	1.000	0.000	1.000	0.681	0.965	3.160	0.112	3.54	17.07% (1.37 σ) [2]
Planck $TT+lowP+H0+BAO$	5.720	1.000	0.000	1.000	0.685	0.967	3.146	0.105	3.87	14.41% (1.46 σ) [2]
Planck $TT, TE, EE+lowP$	6.455	1.000	0.000	1.000	0.673	0.960	3.128	0.094	3.36	18.65% (1.32 σ) [2]
Planck $TT, TE, EE+lowP+H0$	6.835	1.000	0.022	1.000	0.680	0.964	3.134	0.098	3.25	19.73% (1.29 σ) [2]
Planck $TT, TE, EE+lowP+BAO$	6.972	1.000	0.013	1.000	0.678	0.964	3.133	0.097	3.24	19.80% (1.29 σ) [2]
Planck $TT, TE, EE+lowP+H0 + BAO$	6.613	1.000	0.000	1.000	0.681	0.965	3.135	0.099	3.26	19.54% (1.29 σ) [2]

TABLE XVI. Model: **atan3**.

data-set	k_c^{-1} [Gpc]	λ	β	α	h	n_s	$\ln(10^{10}\mathcal{A}_s)$	τ	Γ	γ
Planck TT	1.683	1.000	0.471	0.935	0.699	0.971	3.344	0.203	5.91	11.59% (1.57 σ) [3]
Planck $TT+H0$	1.327	1.000	0.505	1.000	0.712	0.975	3.391	0.227	8.25	4.12% (2.04 σ) [3]
Planck $TT+BAO$	1.981	1.000	0.477	1.000	0.688	0.964	3.305	0.181	5.02	17.02% (1.37 σ) [3]
Planck $TT+H0+BAO$	1.442	1.000	0.502	0.544	0.691	0.969	3.278	0.171	5.78	12.29% (1.54 σ) [3]
Planck $TT+lowP$	3.659	1.000	0.009	0.515	0.676	0.963	3.149	0.105	3.64	30.30% (1.03 σ) [3]
Planck $TT+lowP+H0$	3.560	1.000	0.003	0.501	0.691	0.972	3.168	0.118	4.14	24.62% (1.16 σ) [3]
Planck $TT+lowP+BAO$	5.274	1.000	0.000	1.000	0.681	0.965	3.160	0.112	3.54	31.62% (1.00 σ) [3]
Planck $TT+lowP+H0+BAO$	5.719	1.000	0.000	1.000	0.685	0.967	3.146	0.105	3.88	27.48% (1.09 σ) [3]
Planck $TT, TE, EE+lowP$	6.540	1.000	0.003	0.980	0.673	0.960	3.129	0.094	3.36	33.93% (0.96 σ) [3]
Planck $TT, TE, EE+lowP+H0$	4.823	1.000	0.005	0.511	0.680	0.965	3.123	0.094	3.28	35.00% (0.93 σ) [3]
Planck $TT, TE, EE+lowP+BAO$	4.446	1.000	0.002	0.508	0.677	0.964	3.125	0.094	3.43	33.03% (0.97 σ) [3]
Planck $TT, TE, EE+lowP+H0+BAO$	6.613	1.000	0.000	1.000	0.681	0.965	3.135	0.099	3.28	35.09% (0.93 σ) [3]

similar to those of **atan4**.

Let us evaluate the significance of these fits for the special case **atan1**. Although this model seems to provide fits which are better than for the fiducial case, in some cases with an improvement close to 2.5σ , these fits are actually not reliable because they are unstable with respect to the parameter values obtained. Indeed, when polarization data are added, the parameters change abruptly and, moreover, the significance is reduced, as expected for a statistical fluctuation. Finally, including all data sets, we obtain a marginal 1.8σ significance for a smooth and broad deficit at very large scales.

3. Exponential cut-off models: **expc1-3**

The exponential cut-off models have approximately the same characteristics as the **atan** models discussed above. The main difference is the absence of a transition shape parameter (α), which in any case does not change any of the conclusions for **atan**. For this function, we picked $\lambda = 1/2$ when λ is fixed. This introduces a wider deficit window than for **atan1-2**, explaining why the resulting characteristic scales seem to vary between the two categories of models.

Regarding the significance, we reach the same conclusions as for **atan**, only with a slightly better fit for almost all data sets. This provides another indication that at least two extra parameters are needed, as the improvement stems from having a broader deficit function. This shows that the range over which the deficit function acts needs to be taken into account. An important case is **expc2**, whose equivalent was not tested with **atan**: we allow k_c and λ to vary freely while keeping $\beta = 0$. This case shows that, for a modification at large scales, a wider window is preferred (hence the lower value for λ). The results for **expc3** and **atan4** are very similar, reinforcing our previous conclusion. The fits also naturally lead to a sharp transition at smaller scales. A smooth and broad transition at very large scales is also possible, although only marginally significant.

4. Sharp deficit model: **jump**

The results for this model are summarized in Table XXI. We observe that the parameter values are now consistent across all data sets, although the significance remains marginal and resembles those for **atan1** and **expc2**. In the case of **jump**, however, all data sets point

TABLE XVII. Model: **atan4**.

data-set	k_c^{-1} [Gpc]	λ	β	α	h	n_s	$\ln(10^{10}\mathcal{A}_s)$	τ	Γ	γ
Planck TT	0.357	41.294	0.793	0.577	0.690	0.978	3.254	0.163	6.93	13.95% (1.48 σ) [4]
Planck TT +H0	1.298	1.006	0.506	0.987	0.712	0.975	3.391	0.227	8.31	8.09% (1.75 σ) [4]
Planck TT +BAO	0.350	48.232	0.768	0.506	0.690	0.979	3.294	0.183	5.45	24.40% (1.16 σ) [4]
Planck TT +H0+BAO	0.348	45.708	0.766	0.524	0.691	0.979	3.295	0.184	6.54	16.24% (1.40 σ) [4]
Planck TT +lowP	0.376	37.218	0.805	0.511	0.676	0.967	3.147	0.106	5.02	28.56% (1.07 σ) [4]
Planck TT +lowP+H0	0.379	40.773	0.813	0.564	0.687	0.973	3.153	0.111	4.69	32.01% (0.99 σ) [4]
Planck TT +lowP+BAO	0.371	45.702	0.816	0.520	0.682	0.971	3.154	0.110	4.57	33.45% (0.97 σ) [4]
Planck TT +lowP+H0+BAO	0.375	42.398	0.820	0.521	0.686	0.972	3.153	0.111	4.95	29.28% (1.05 σ) [4]
Planck TT , TE, EE+lowP	0.375	31.287	0.824	0.699	0.672	0.964	3.120	0.091	5.73	22.03% (1.23 σ) [4]
Planck TT , TE, EE+lowP+H0	0.391	31.476	0.821	0.765	0.680	0.968	3.131	0.099	5.49	24.10% (1.17 σ) [4]
Planck TT , TE, EE+lowP+BAO	0.371	31.684	0.820	0.675	0.678	0.968	3.135	0.101	5.53	23.68% (1.18 σ) [4]
Planck TT , TE, EE+lowP+H0+BAO	0.389	31.581	0.817	0.761	0.680	0.968	3.134	0.100	5.43	24.56% (1.16 σ) [4]

TABLE XVIII. Model: **expcl**.

data-set	k_c^{-1} [Gpc]	λ	β	α	h	n_s	$\ln(10^{10}\mathcal{A}_s)$	τ	Γ	γ
Planck TT	2.094	0.500	0.000	-	0.694	0.979	3.286	0.180	5.61	1.78% (2.37 σ) [1]
Planck TT +H0	1.465	0.500	0.000	-	0.710	0.987	3.366	0.223	6.93	0.85% (2.63 σ) [1]
Planck TT +BAO	2.232	0.500	0.000	-	0.685	0.974	3.260	0.164	5.30	2.14% (2.30 σ) [1]
Planck TT +H0+BAO	2.106	0.500	0.000	-	0.691	0.977	3.282	0.177	5.75	1.65% (2.40 σ) [1]
Planck TT +lowP	2.894	0.500	0.000	-	0.676	0.966	3.156	0.110	3.85	4.99% (1.96 σ) [1]
Planck TT +lowP+H0	3.237	0.500	0.000	-	0.690	0.974	3.161	0.116	3.99	4.58% (2.00 σ) [1]
Planck TT +lowP+BAO	2.974	0.500	0.000	-	0.681	0.969	3.158	0.113	3.84	5.00% (1.96 σ) [1]
Planck TT +lowP+H0+BAO	3.074	0.500	0.000	-	0.685	0.971	3.156	0.113	4.22	4.00% (2.05 σ) [1]
Planck TT , TE, EE+lowP	3.390	0.500	0.000	-	0.673	0.965	3.138	0.100	4.04	4.45% (2.01 σ) [1]
Planck TT , TE, EE+lowP+H0	3.671	0.500	0.000	-	0.680	0.969	3.141	0.104	4.13	4.21% (2.03 σ) [1]
Planck TT , TE, EE+lowP+BAO	3.503	0.500	0.000	-	0.677	0.967	3.139	0.102	4.10	4.28% (2.03 σ) [1]
Planck TT , TE, EE+lowP+H0+BAO	3.671	0.500	0.000	-	0.681	0.969	3.137	0.102	3.98	4.62% (1.99 σ) [1]

in the same general direction and parameter values that provide a good fit for one data set also provide a good

fit for the others. This means that, to have a hope of measuring an effect using the full range of data sets, we need to consider the **jump** model.

-
- [1] P. Peter and J.-P. Uzan, *Primordial Cosmology*, Oxford Graduate Texts (Oxford University Press, 2013), ISBN 9780199665150, 9780199209910.
- [2] D. J. Schwarz, C. J. Copi, D. Huterer, and G. D. Starkman, *Class. Quant. Grav.* **33**, 184001 (2016), 1510.07929.
- [3] J. Chluba, J. Hamann, and S. P. Patil, *Int. J. Mod. Phys. D24*, 1530023 (2015), 1505.01834.
- [4] P. A. R. Ade et al. (Planck), *Astron. Astrophys.* **594**, A20 (2016), 1502.02114.
- [5] I.-C. Wang and K.-W. Ng, *Phys. Rev. D77*, 083501 (2008), 0704.2095.
- [6] S. Colin and A. Valentini, *Phys. Rev. D92*, 043520 (2015), 1407.8262.
- [7] S. Colin and A. Valentini, *Int. J. Mod. Phys. D25*, 1650068 (2016), 1510.03508.
- [8] S. Colin and A. Valentini, *Phys. Rev. D88*, 103515 (2013), 1306.1579.
- [9] A. Valentini, *Phys. Rev. D82*, 063513 (2010), 0805.0163.
- [10] P. Peter and N. Pinto-Neto, *Phys. Rev. D78*, 063506 (2008), 0809.2022.
- [11] D. Battfeld and P. Peter, *Phys. Rep.* **571**, 1 (2015), 1406.2790.
- [12] R. Brandenberger and P. Peter, *Found. Phys.* **47**, 797 (2017), 1603.05834.
- [13] Planck Collaboration, P. A. R. Ade, N. Aghanim, C. Armitage-Caplan, M. Arnaud, M. Ashdown, F. Atrio-Barandela, J. Aumont, C. Baccigalupi, A. J. Banday, et al., *Astron. Astrophys.* **571**, A22 (2014), 1303.5082.
- [14] Planck Collaboration, P. A. R. Ade, N. Aghanim, M. Arnaud, F. Arroja, M. Ashdown, J. Aumont, C. Baccigalupi, M. Ballardini, A. J. Banday, et al., *Astron. Astrophys.* **594**, A20 (2016), 1502.02114.
- [15] C. R. Contaldi, M. Peloso, L. Kofman, and A. Linde, *J. Cosmol. Astropart. Phys.* **7**, 002 (2003), astro-ph/0303636.
- [16] Planck Collaboration, P. A. R. Ade, N. Aghanim, C. Armitage-Caplan, M. Arnaud, M. Ashdown, F. Atrio-Barandela, J. Aumont, C. Baccigalupi, A. J. Banday, et al., *Astron. Astrophys.* **571**, A16 (2014), 1303.5076.

TABLE XIX. Model: **expc2**.

data-set	$k_c^{-1}[\text{Gpc}]$	λ	β	α	h	n_s	$\ln(10^{10}\mathcal{A}_s)$	τ	Γ	γ
Planck TT	2.687	0.439	0.000	-	0.692	0.977	3.276	0.174	5.84	5.40% (1.93 σ) [2]
Planck $TT+H0$	1.624	0.360	0.000	-	0.716	0.977	3.410	0.241	8.55	1.39% (2.46 σ) [2]
Planck $TT+BAO$	2.532	0.448	0.000	-	0.685	0.972	3.261	0.165	5.50	6.40% (1.85 σ) [2]
Planck $TT+H0+BAO$	2.498	0.439	0.000	-	0.690	0.976	3.281	0.176	6.03	4.91% (1.97 σ) [2]
Planck $TT+lowP$	2.700	0.515	0.000	-	0.676	0.966	3.155	0.110	3.87	14.44% (1.46 σ) [2]
Planck $TT+lowP+H0$	2.722	0.569	0.000	-	0.691	0.975	3.159	0.116	4.07	13.05% (1.51 σ) [2]
Planck $TT+lowP+BAO$	2.974	0.527	0.000	-	0.681	0.969	3.145	0.107	3.88	14.40% (1.46 σ) [2]
Planck $TT+lowP+H0+BAO$	3.074	0.500	0.000	-	0.685	0.971	3.156	0.113	4.22	12.13% (1.55 σ) [2]
Planck $TT, TE, EE+lowP$	2.742	0.574	0.000	-	0.674	0.965	3.134	0.099	4.16	12.51% (1.53 σ) [2]
Planck $TT, TE, EE+lowP+H0$	2.824	0.582	0.000	-	0.681	0.969	3.139	0.103	4.16	12.48% (1.53 σ) [2]
Planck $TT, TE, EE+lowP+BAO$	2.766	0.588	0.000	-	0.679	0.968	3.137	0.101	4.13	12.65% (1.53 σ) [2]
Planck $TT, TE, EE+lowP+H0+BAO$	2.589	0.605	0.000	-	0.682	0.970	3.147	0.107	4.31	11.58% (1.57 σ) [2]

TABLE XX. Model: **expc3**.

data-set	$k_c^{-1}[\text{Gpc}]$	λ	β	α	h	n_s	$\ln(10^{10}\mathcal{A}_s)$	τ	Γ	γ
Planck TT	0.334	14.068	0.782	-	0.691	0.979	3.273	0.173	6.73	8.12% (1.74 σ) [3]
Planck $TT+H0$	1.606	0.362	0.007	-	0.716	0.978	3.410	0.241	8.56	3.57% (2.10 σ) [3]
Planck $TT+BAO$	0.333	19.941	0.787	-	0.685	0.975	3.254	0.162	6.68	8.28% (1.73 σ) [3]
Planck $TT+H0+BAO$	0.332	17.363	0.768	-	0.690	0.979	3.289	0.181	6.55	8.76% (1.71 σ) [3]
Planck $TT+lowP$	0.353	13.593	0.799	-	0.676	0.967	3.154	0.109	4.71	19.42% (1.30 σ) [3]
Planck $TT+lowP+H0$	0.360	14.399	0.809	-	0.688	0.974	3.166	0.118	4.53	20.97% (1.25 σ) [3]
Planck $TT+lowP+BAO$	0.353	17.005	0.804	-	0.681	0.970	3.165	0.116	4.37	22.42% (1.22 σ) [3]
Planck $TT+lowP+H0+BAO$	0.356	15.636	0.805	-	0.686	0.972	3.165	0.117	4.72	19.34% (1.30 σ) [3]
Planck $TT, TE, EE+lowP$	0.349	13.077	0.817	-	0.673	0.965	3.130	0.096	5.70	12.72% (1.53 σ) [3]
Planck $TT, TE, EE+lowP+H0$	0.357	13.664	0.819	-	0.679	0.968	3.140	0.103	5.46	14.12% (1.47 σ) [3]
Planck $TT, TE, EE+lowP+BAO$	0.352	14.002	0.812	-	0.679	0.968	3.137	0.101	5.39	14.52% (1.46 σ) [3]
Planck $TT, TE, EE+lowP+H0+BAO$	0.356	13.829	0.815	-	0.680	0.968	3.136	0.101	5.33	14.90% (1.44 σ) [3]

- [17] Planck Collaboration, P. A. R. Ade, N. Aghanim, M. Arnaud, M. Ashdown, J. Aumont, C. Baccigalupi, A. J. Banday, R. B. Barreiro, J. G. Bartlett, et al., *Astron. Astrophys.* **594**, A13 (2015), 1502.01589.
- [18] A. G. Riess, L. M. Macri, S. L. Hoffmann, D. Scolnic, S. Casertano, A. V. Filippenko, B. E. Tucker, M. J. Reid, D. O. Jones, J. M. Silverman, et al., *Astrophys. J.* **826**, 56 (2016), 1604.01424.
- [19] F. Beutler, C. Blake, M. Colless, D. H. Jones, L. Staveley-Smith, L. Campbell, Q. Parker, W. Saunders, and F. Watson, *Mon. Not. R. Astron. Soc.* **416**, 3017 (2011), 1106.3366.
- [20] A. J. Ross, L. Samushia, C. Howlett, W. J. Percival, A. Burden, and M. Manera, *Mon. Not. Roy. Astron. Soc.* **449**, 835 (2015), 1409.3242.
- [21] S. Alam, M. Ata, S. Bailey, F. Beutler, D. Bizyaev, J. A. Blazek, A. S. Bolton, J. R. Brownstein, A. Burden, C.-H. Chuang, et al., *Mon. Not. R. Astron. Soc.* **470**, 2617 (2017), 1607.03155v1.
- [22] M. Ata, F. Baumgarten, J. Bautista, F. Beutler, D. Bizyaev, M. R. Blanton, J. A. Blazek, A. S. Bolton, J. Brinkmann, J. R. Brownstein, et al., *Mon. Not. R. Astron. Soc.* **473**, 4773 (2018), 1705.06373.
- [23] T. Delubac, J. E. Bautista, N. G. Busca, J. Rich, D. Kirkby, S. Bailey, A. Font-Ribera, A. Slosar, K.-G. Lee, M. M. Pieri, et al., *Astron. Astrophys.* **574**, A59 (2015), 1404.1801.
- [24] A. Font-Ribera, D. Kirkby, N. Busca, J. Miralda-Escudé, N. P. Ross, A. Slosar, J. Rich, É. Aubourg, S. Bailey, V. Bhardwaj, et al., *J. Cosmol. Astropart. Phys.* **5**, 027 (2014), 1311.1767.
- [25] J. Muir, S. Adhikari, and D. Huterer, *Phys. Rev.* **D98**, 023521 (2018), 1806.02354.
- [26] H. Craig, *Introduction to Mathematical Statistics* (Prentice Hall, 1984).
- [27] P. G. Hoel, *Introduction to Mathematical Statistics* (John Wiley & Sons, 2003).
- [28] A. van der Vaart, *Asymptotic Statistics*, Cambridge Series in Statistical and Probabilistic Mathematics (Cambridge University Press, 2000), ISBN 9780521784504.
- [29] J. Goodman and J. Weare, *CAMCoS* **5**, 65 (2010).
- [30] D. Foreman-Mackey, D. W. Hogg, D. Lang, and J. Goodman, *Publications of the Astronomical Society of the Pacific* **125**, 306 (2013).
- [31] D. Blas, J. Lesgourgues, and T. Tram, *J. Cosmol. Astropart. Phys.* **2011**, 034 (2011).
- [32] J. Lesgourgues, *ArXiv e-prints* (2011), 1104.2934.
- [33] J. Lesgourgues and T. Tram, *J. Cosmol. Astropart. Phys.* **9**, 032 (2011), 1104.2935.
- [34] Planck Collaboration, P. A. R. Ade, N. Aghanim, M. Arnaud, F. Arroja, M. Ashdown, J. Aumont, C. Baccigalupi, M. Ballardini, A. J. Banday, et al., *ArXiv e-prints* (2015), 1502.02114.
- [35] A. Valentini (2015), 1510.02523.

TABLE XXI. Model: **jump**.

data-set	k_c^{-1} [Gpc]	λ	β	α	h	n_s	$\ln(10^{10} \mathcal{A}_s)$	τ	Γ	γ
Planck TT	0.357	-	0.781	-	0.686	0.976	3.261	0.166	6.77	3.39% (2.12 σ) [2]
Planck TT +H0	0.353	-	0.763	-	0.704	0.988	3.326	0.203	7.17	2.77% (2.20 σ) [2]
Planck TT +BAO	0.361	-	0.790	-	0.684	0.975	3.252	0.161	6.76	3.40% (2.12 σ) [2]
Planck TT +H0+BAO	0.354	-	0.769	-	0.690	0.979	3.287	0.180	6.70	3.50% (2.11 σ) [2]
Planck TT +lowP	0.372	-	0.811	-	0.676	0.967	3.145	0.105	5.06	7.97% (1.75 σ) [2]
Planck TT +lowP+H0	0.374	-	0.813	-	0.690	0.975	3.166	0.119	4.61	9.99% (1.65 σ) [2]
Planck TT +lowP+BAO	0.370	-	0.798	-	0.682	0.971	3.170	0.119	4.35	11.37% (1.58 σ) [2]
Planck TT +lowP+H0+BAO	0.373	-	0.807	-	0.686	0.973	3.169	0.119	4.76	9.24% (1.68 σ) [2]
Planck TT, TE, EE +lowP	0.380	-	0.816	-	0.673	0.964	3.122	0.093	5.79	5.53% (1.92 σ) [2]
Planck TT, TE, EE +lowP+H0	0.385	-	0.825	-	0.680	0.968	3.124	0.095	5.30	7.07% (1.81 σ) [2]
Planck TT, TE, EE +lowP+BAO	0.382	-	0.829	-	0.678	0.967	3.118	0.093	5.30	7.08% (1.81 σ) [2]
Planck TT, TE, EE +lowP+H0+BAO	0.381	-	0.832	-	0.681	0.969	3.124	0.095	5.14	7.66% (1.77 σ) [2]

- [36] H. Jeffreys, *The Theory of Probability*, Oxford Classic Texts in the Physical Sciences (OUP Oxford, 1998), ISBN 9780191589676.
- [37] R. Trotta, Mon. Not. R. Astron. Soc. **378**, 72 (2007), astro-ph/0504022.
- [38] S. D. P. Vitenti and M. Penna-Lima, *Numerical cosmology - NumCosmo*, Astrophysics Source Code Library (2014), 1408.013, URL <https://github.com/NumCosmo/NumCosmo>.
- [39] S. G. Johnson, *The nlopt nonlinear-optimization package* (2014).
- [40] J. A. Nelder and R. Mead, Comput. J. **7**, 308 (1965).
- [41] M. J. Box, Comput. J. **8**, 42 (1965).
- [42] J. A. Richardson and J. L. Kuester, Commun. ACM **16**, 487 (1973), ISSN 0001-0782.
- [43] T. H. Rowan, Tech. Rep., University of Texas at Austin (1990).
- [44] A. Lewis, A. Challinor, and A. Lasenby, Astrophys. J. **538**, 473 (2000), astro-ph/9911177.
- [45] A. Lewis, Phys. Rev. D **87**, 103529 (2013).
- [46] M. J. D. Powell (2009), URL http://www.damtp.cam.ac.uk/user/na/NA_papers/NA2009_06.pdf.
- [47] C. Doux, M. Penna-Lima, S. D. P. Vitenti, J. Tréguer, E. Aubourg, and K. Ganga, Mon. Not. R. Astron. Soc. **480**, 5386 (2018), 1706.04583, URL <http://adsabs.harvard.edu/abs/2018MNRAS.480.5386D>.
- [48] M. D. Weinberg, Bayesian Anal. **7**, 737 (2012), URL <https://doi.org/10.1214/12-BA725>.